AD-A126 000 FORMULATION OF A PROTOTYPE COUPLED ATMOSPHERIC AND OCEANIC BOUNDARY LAYER MODEL(U) NAVAL POSTGRADUATE SCHOOL MONTEREY CA M C O'LOUGHLIN DEC 82 1/1

UNCLASSIFIED F/G 8/10 NL

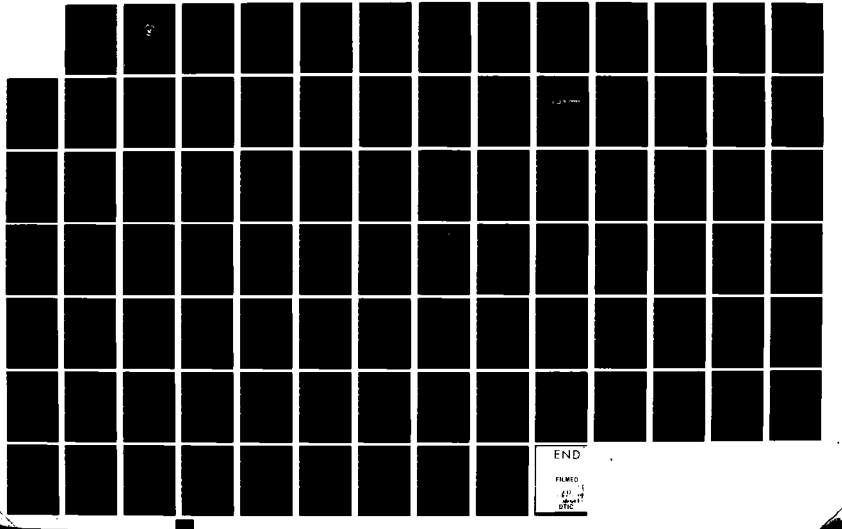

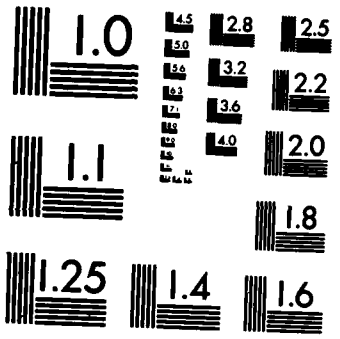

MICROCOPY RESOLUTION TEST CHART
NATIONAL BUREAU OF STANDARDS-1963-A

NAVAL POSTGRADUATE SCHOOL
Monterey, California

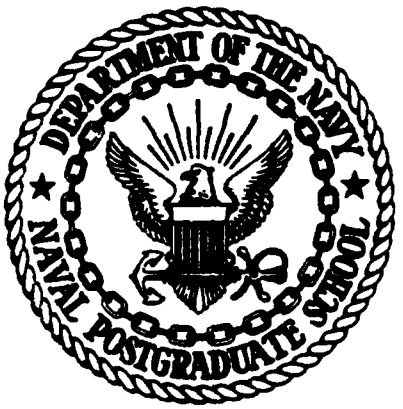

THESIS

FORMULATION OF A PROTOTYPE COUPLED ATMOSPHERIC AND OCEANIC BOUNDARY LAYER MODEL

by

Michael Charles O'Loughlin

December 1982

Thesis Advisor: K.L. Davidson

Approved for public release; distribution unlimited

SECURITY CLASSIFICATION OF THIS PAGE (When Data Entered)

REPORT DOCUMENTATION PAGE		READ INSTRUCTIONS BEFORE COMPLETING FORM
1. REPORT NUMBER	2. GOVT ACCESSION NO. AD-A126 400	3. RECIPIENT'S CATALOG NUMBER
4. TITLE (and Subtitle) Formulation of a Prototype Coupled Atmospheric and Oceanic Boundary Layer Model		5. TYPE OF REPORT & PERIOD COVERED Master's Thesis December 1982
		6. PERFORMING ORG. REPORT NUMBER
7. AUTHOR(s) Michael Charles O'Loughlin		8. CONTRACT OR GRANT NUMBER(s)
9. PERFORMING ORGANIZATION NAME AND ADDRESS Naval Postgraduate School Monterey, California 93940		10. PROGRAM ELEMENT, PROJECT, TASK AREA & WORK UNIT NUMBERS
11. CONTROLLING OFFICE NAME AND ADDRESS Naval Postgraduate School Monterey, California 93940		12. REPORT DATE December 1982
		13. NUMBER OF PAGES 90
14. MONITORING AGENCY NAME & ADDRESS(if different from Controlling Office) Naval Postgraduate School Monterey, California 93940		15. SECURITY CLASS. (of this report) Unclassified
		15a. DECLASSIFICATION/DOWNGRADING SCHEDULE

16. DISTRIBUTION STATEMENT (of this Report)

Approved for public release; distribution unlimited

17. DISTRIBUTION STATEMENT (of the abstract entered in Block 20, if different from Report)

18. SUPPLEMENTARY NOTES

19. KEY WORDS (Continue on reverse side if necessary and identify by block number)

Marine Atmospheric Boundary Layer, Oceanic Boundary Layer, Coupled Boundary Layer Model, interface, well-mixed layers, inversion, thermocline, entrainment surface turbulent fluxes, radiation, sea-surface temperature, cloud formation, cloud dissipation

20. ABSTRACT (Continue on reverse side if necessary and identify by block number)

A prototype coupled Marine Atmospheric Boundary Layer (MABL) and Oceanic Boundary Layer (OBL), from physical models which have been separately formulated, is developed. The observational efforts will be directed toward coupling (local) point MABL and OBL features. Emphasis in the characterization of local features will be on the evolutions of the adjacent well-mixed layers. The approach will be to compare observed evolutions in the oceanic and atmospheric boundary layers with predictions from bulk models wherein the ocean influences the atmosphere through the surface temperature which, in turn, is influenced by atmospheric

DD FORM 1 JAN 73 1473 EDITION OF 1 NOV 68 IS OBSOLETE
S/N 0102-014-6601

SECURITY CLASSIFICATION OF THIS PAGE (When Data Entered)

forcing. The atmospheric forcing parameters are the local surface turbulent fluxes and radiation. Surface turbulent fluxes are controlled by the surface temperature and atmospheric mixed layer parameters. Radiation is controlled by predicted cloud formation and dissipation.

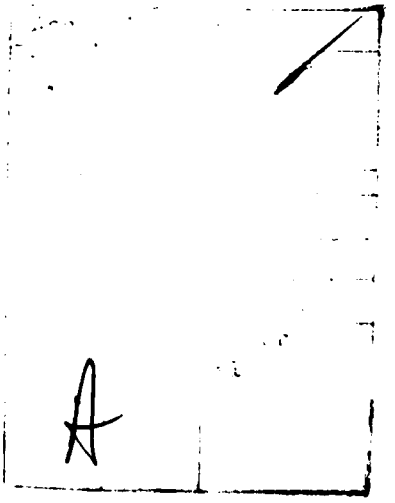

Approved for public release; distribution unlimited

Formulation of a Prototype Coupled Atmospheric and Oceanic Boundary Layer Model

by

Michael C. O'Loughlin
Lieutenant, United States Navy
B.S., United States Naval Academy, 1976

Submitted in partial fulfillment of the requirements for the degree of

MASTER OF SCIENCE IN METEOROLOGY AND OCEANOGRAPHY

from the

NAVAL POSTGRADUATE SCHOOL
December 1982

Author: Michael C O'Loughlin

Approved by: Kenneth L Davidson
Thesis Advisor

Roland W Garwood Jr
Second Reader

Chairman, Department of Meteorology

Dean of Science and Engineering

ABSTRACT

A prototype coupled Marine Atmospheric Boundary Layer (MABL) and Oceanic Boundary Layer (OBL) model, from physical models which have been separately formulated, is developed. The observational efforts will be directed toward coupling (local) point MABL and OBL features. Emphasis in the characterization of local features will be on the evolutions of the adjacent well-mixed layers. The approach will be to compare observed evolutions in the oceanic and atmospheric boundary layers with predictions from bulk models wherein the ocean influences the atmosphere through the surface temperature which, in turn, is influenced by atmospheric forcing. The atmospheric forcing parameters are the local surface turbulent fluxes and radiation. Surface turbulent fluxes are controlled by the surface temperature and atmospheric mixed layer parameters. Radiation is controlled by predicted cloud formation and dissipation.

TABLE OF CONTENTS

LIST OF TABLES

LIST OF FIGURES

ACKNOWLEDGEMENT

The author wishes to thank Professor K.L. Davidson, Department of Meteorology, and Dr. R.W. Garwood, Department of Oceanography, Naval Postgraduate School, for their time, interest and guidence throughout this study, Dr. C.W. Fairall for his helpful discussions and review of this thesis, and to CDR J.J. Jensen who provided motivation for this effort. Particular appreciation is extended to Peter Guest for his assistance in programing and research.

Finally, I would like to express my gratitude to my wife, Stephanie, and to my two daughters, Jamie and Lorry, for their patience, understanding and support during the two years of study.

I. INTRODUCTION

The idea that both atmospheric and subsurface environmental conditions can have a significant effect (enhancement or degradation) on modern weapon and sensor systems has now become a reality to many military leaders. This has led to a greater demand for more reliable and accurate atmospheric and oceanic prediction schemes. Prediction of the existence and evolution of electromagnetic ducts are important in predicting over the horizon surface to surface detection. Predictions of the inversion height is important where it is known that optical propagation is degraded due to turbulence and extinction. Ocean mixed layer predictions are important for determining convergence zone distances, optimum source level depth, and cutoff frequency for acoustic surface duct propagation.

The ability to provide accurate forecasts requires a complete understanding of the dynamical processes occurring in each of the atmospheric and oceanic boundary layers, and as important, the processes associated with coupled local changes in the two layers.

Very little is known about the interactive nature of the adjacent turbulent boundary layers. The objective of this

thesis is to formulate a model which couples two already existing and proven models for the respective adjacent well-mixed boundary layers. This coupling is achieved by matching the surface boundary conditions for stress, mass flux and heat flux (Figure 1).

This coupled model may then be used to examine the processes of coupled local oceanic and atmospheric mixed layers at time and spatial scales of 12-18 hours and 50-100 km, respectively. Significant changes in both mixed layers can occur at these scales. Explaining these changes requires coupled evaluations of existing atmospheric and oceanic well-mixed layers at a point.

At the present time, we only have qualitative evidence that changes in each layer are correlated. The rigorous specifications or descriptions of the coupling will require considerable interpretive efforts and, perhaps, improved formulation of the separate models.

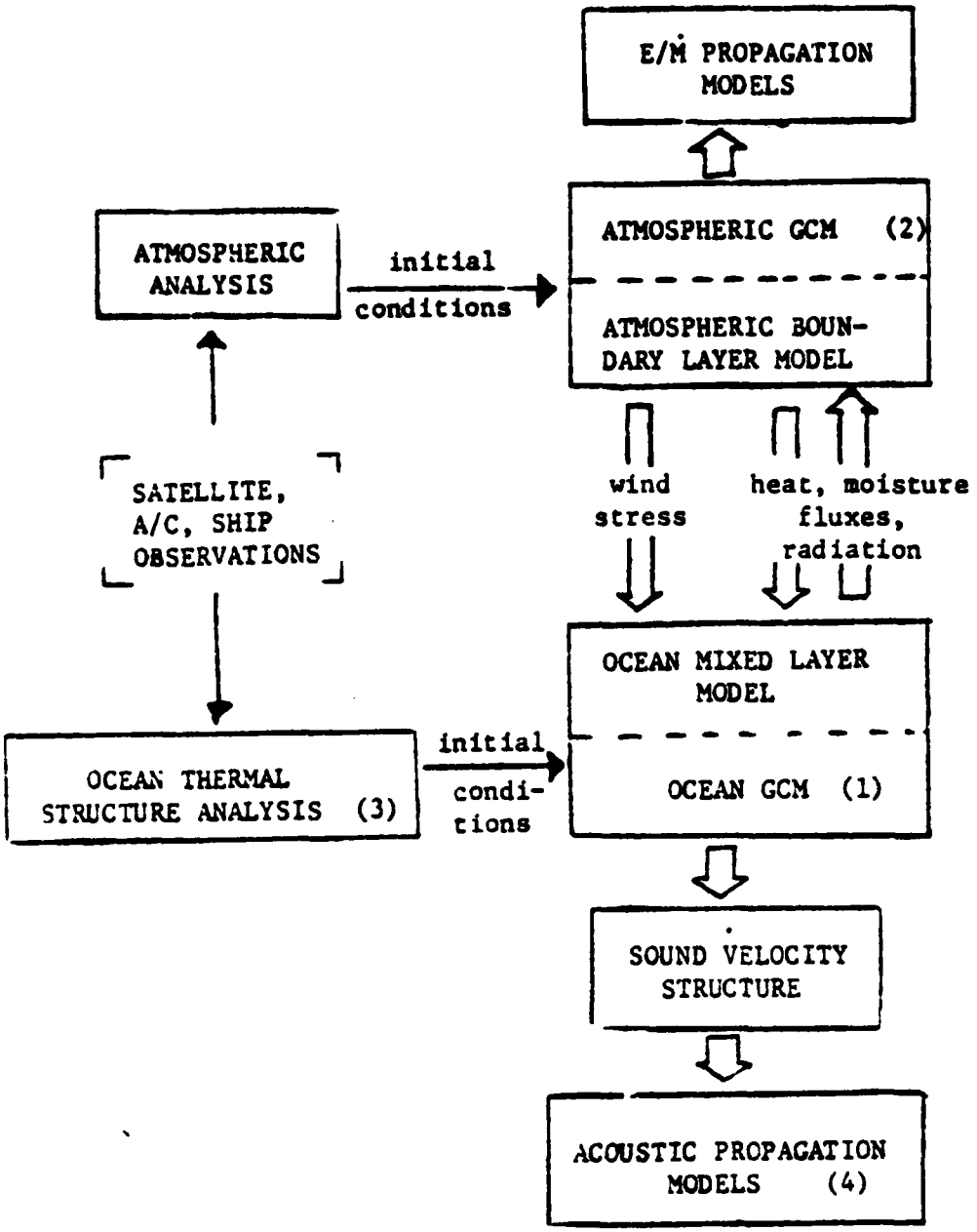

Figure 1. Coupled Environmental Model System (1) Embedded mixed layer in OCGM (Adamec, et al, 1981) or TOPS (2) NOGAPS/NORAPS or 1-D model with prescribed subsidence (3) EOTS or other (4) At FNOC or ICAPS/SIMIS, ect.

II. BACKGROUND

A. GENERAL BOUNDARY LAYER FEATURES

The Marine Atmospheric Boundary Layer (MABL) extends from the surface through the capping inversion. The Oceanic Boundary Layer (OBL) extends from the surface to the seasonal thermocline. The air-sea interface is bordered by oceanic and atmospheric turbulent mixed layers which effectively insulate the quasi-geostrophic oceanic and atmospheric flows below the thermocline and above the inversion, respectively. The primary source of the turbulence is the velocity (current) and buoyancy (density) gradients created by interaction at the interface. The large vertical mixing yields nearly homogeneous (well-mixed) wind, temperature and humidity profiles above the surface. In the ocean, the term mixed layer refers to the region of vertical uniformity in mean velocity and density. Although density is a function of both temperature and salinity, it is usually dependent upon temperature except when large near-surface salinity changes occur due to heavy precipitation or ice melt in high latitudes. At the bottom of the ocean mixed layer and at

the top of the atmosphere mixed layer are thin transition regions (thermocline or inversion). The mixed layers interact with the upper and lower layers at these regions by means of turbulent forced entrainment. Typical model profiles depicting the boundary layer regions for both the atmosphere and ocean are shown in Figure 2.

The well-mixed nature of both the turbulent MABL and OBL implies features for the vertical distribution of mean values and vertical fluxes of wind, temperature and humidity in the atmosphere and density and momentum in the ocean. One feature is that the properties which are conserved during mixing can be treated as being constant with height (depth) in the boundary layer. A second feature is that vertical fluxes of the well-mixed parameters vary linearly with height. These features enable predictions to be based solely on the surface and inversion (entrainment) fluxes if advection is negligible.

Another important source of energy, in addition to turbulent kinetic energy, in both mixed layers is radiation. Unlike the MABL, most of the solar radiation does not penetrate the OBL. Therefore, downward turbulent heat flux in the OBL is as important as the upward flux. Since the long

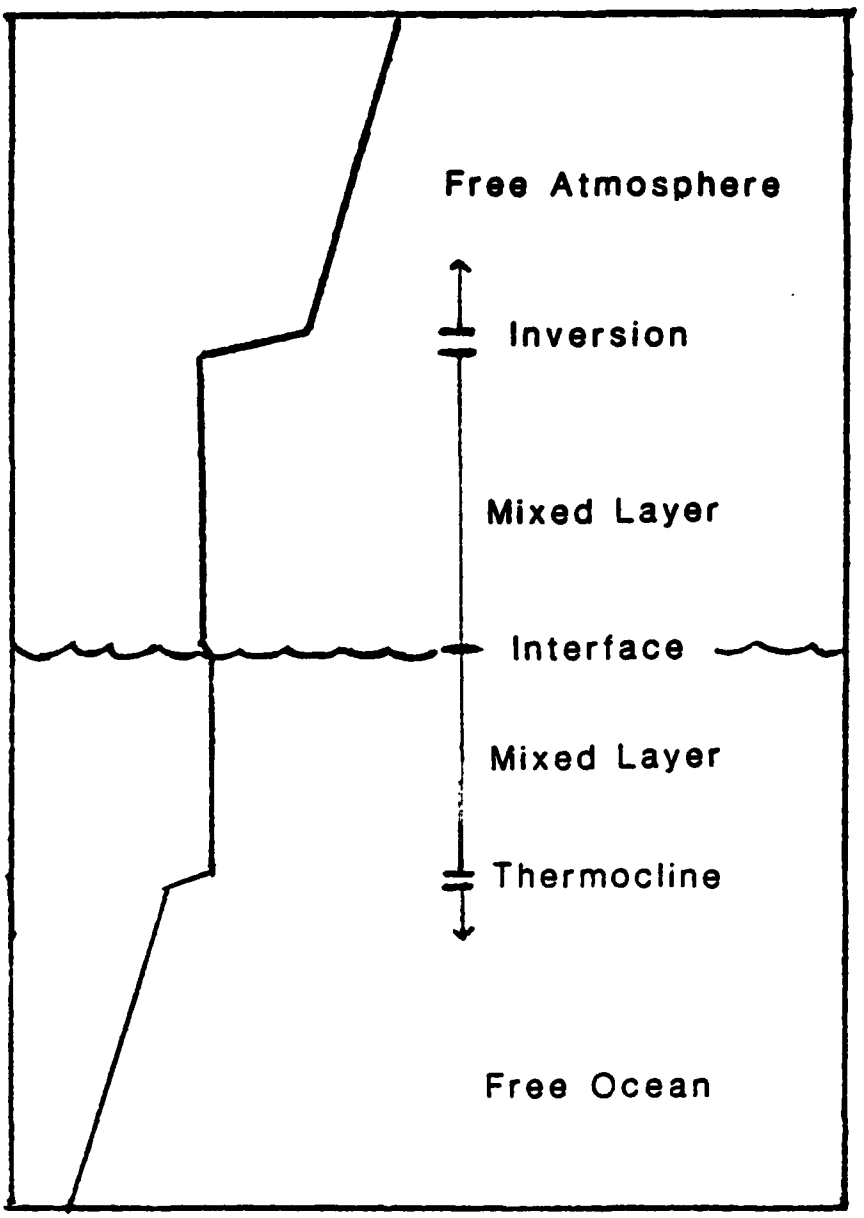

Figure 2. Simplified Atmospheric and Oceanic Boundary Layer Temperature Profiles.

wave (infrared) radiation flux is absorbed and emitted within the first millimeter of the sea surface, this flux component is essentially another component of the oceanic surface heat flux. The total surface heat flux is comprised of sensible and latent heat and the long and short wave solar radiation. Both the long and short wave (solar) fluxes into the ocean are critically dependent upon the existance of clouds in the atmosphere.

In both the MABL and OBL, buoyantly-created velocity fluctuations and mixing have the most pronounced effect on mixed layer characteristics. Garwood (1977) states that buoyancy-forced vertical mixing has a more obvious and direct role in the mechanical energy budget, as shown in Figure 3. In the atmosphere, even under near neutral conditions, buoyancy forced fluctuations and mixing can be quite large. These buoyancy driven energetic eddies fill the atmospheric boundary layer from the surface to the inversion where they entrain warm, dry air and bring more momentum into the mixed layer. If entrainment causes the MABL to extend above the lifting condensation level, clouds or fog will form within the layer.

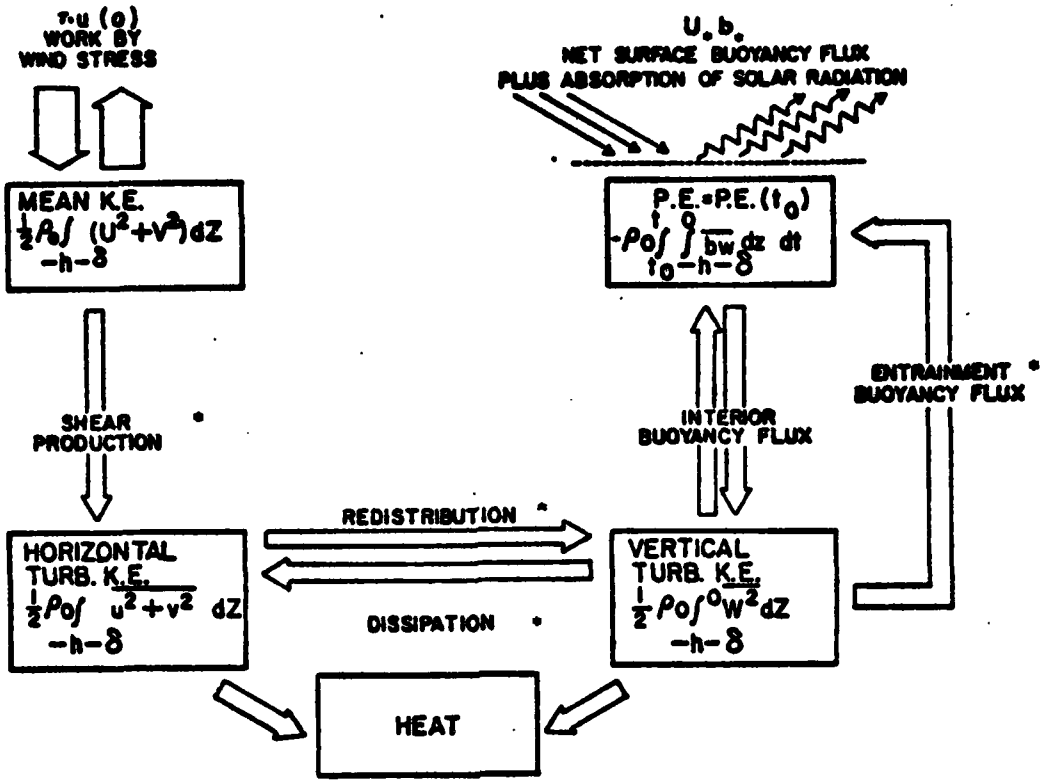

Figure 3. Mechanical Energy Budget for the Ocean Mixed Layer.

It is the realization that buoyancy driven entrainment depends on the near surface stability, which in turn is controlled by local atmospheric forcing of the upper ocean layer which makes a coupled prediction approach necessary. A circularity in cause and effect arises because surface buoyancy flux induced entrainment not only increases the depth of the MABL, but it also changes its effect on the ocean mixed layer. The role of the surface buoyancy flux means changes in the oceanic well-mixed layer could be either the cause or the result of entrainment. Another

cause and effect relationship is the formation and dissipation of clouds within the ABL. Clouds can be caused by changes of the ocean surface temperature. In turn, clouds have a profound effect on the short and long wave radiation budget for the OBL.

These cause and effect relationships show that the assessment of relative roles of dynamic processes in both layers requires coupled evaluations using relatively complex physical models. A data set collected (Davidson et al 1983) over a 48 hour period in May 1978 demonstrates the nature of coupled local changes in the atmospheric and oceanic boundary layers. For a period from 1700 to 0500 local time, clouds existed in the MABL and winds increased steadily from 6 to 9 ms^{-1} during this period. It is suggested this increase was associated with deepening of the MABL (and therefore, the entrainment of additional momentum into the mixed layer) which is, in turn, associated with the surface temperature. The oceanic boundary layer deepened as the wind reached a maximum, resulting in the surface temperature dropping from 14.5° to 13.0°C.

There were other atmospheric response and forcing features observed during the entire 48 hour period from

5/19/1200 to 5/21/1200 PST which are believed to have been associated with coupling between the two layers. Atmospheric and oceanic mixed layer observations appear in Figure 4.

These additional features are:

a) The ABL depth increased from 250 to 750 meters over the 48 hour period. The changes occured in relatively short intervals, from 20/0000 to 20/0400, and from 21/0000 to 21/0500. The ABL depth remained at near constant depths during the intervening 12 to 18 hour periods.

b) The surface layer temperature increase from 20/0000 to 20/1500 is indicative of entrainment of overlying warm air. This entrainment presumably was a factor in the wind speed increase over the same period. The speed increase, in turn, presumably caused the warm shallow OBL to be destroyed which dropped the surface temperature after 20/1800.

c) The most dramatic change in the MABL occured during the period from 21/0000 to 21/0500 which was immediately after the surface temperature had dropped due to wind mixing.

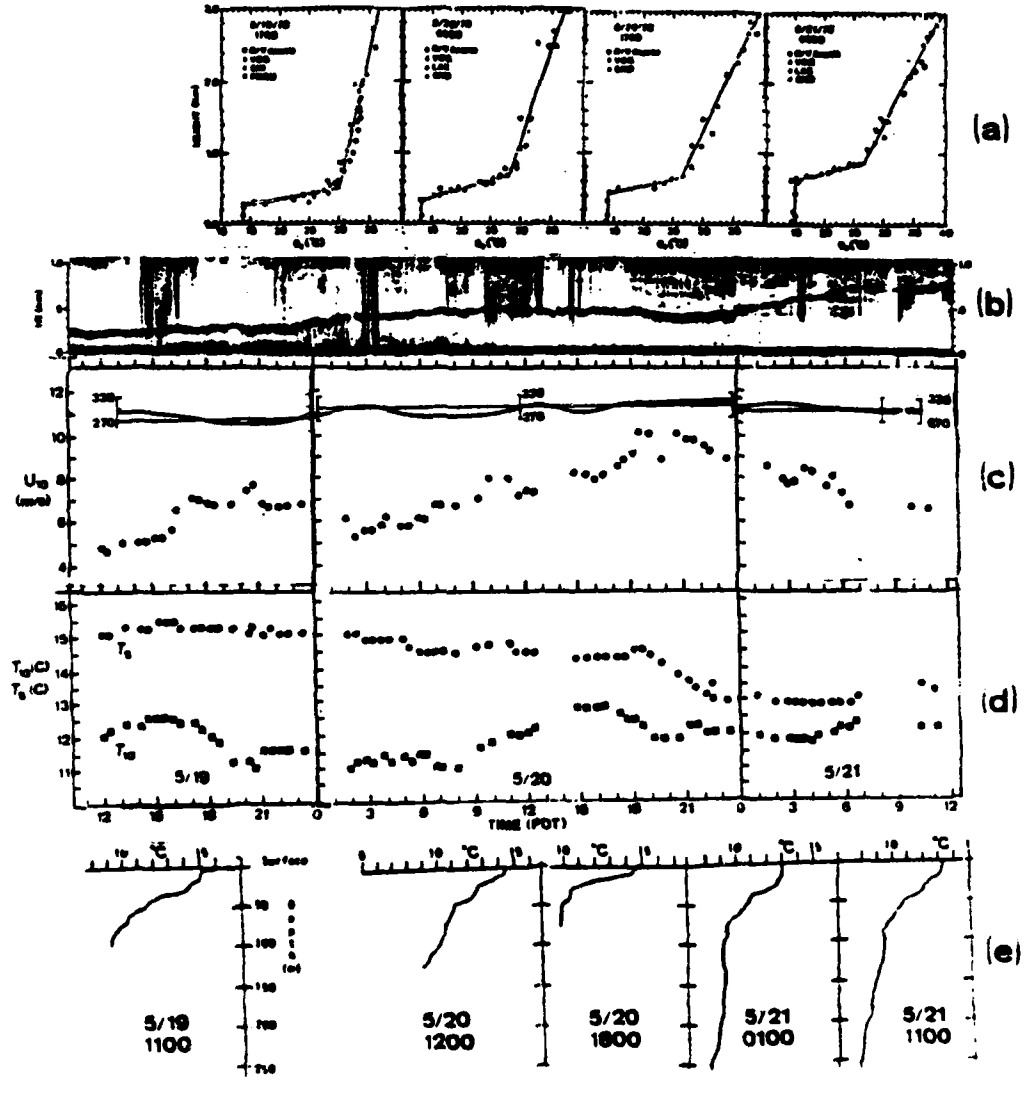

Figure 4. Atmospheric and Oceanic Mixed Layer Observations during CEWCOM-78. (a) potential temperature profiles (b) acoustic sounder record (c) 10 meter wind speed (d) 10 meter and surface temperature and (e) XBT traces.

Questions which could be posed on the basis of the above data are:

a) Did the dramatic change in the ABL depth at 21/0000 occur as a result of the ocean forcing the atmosphere?

b) Does the fact that the mixed layer evolved with rapid changes followed by equilibrium periods indicate feedback between the boundaries?

c) What would have occurred if the wind had reached its maximum value at a time other than after sunset?

d) Was the time of occurrence of the wind maximum and, hence, the ocean mixing controlled by the coupled mixed layer system?

This thesis will attempt to answer some of these questions on the basis of the formulated coupled model. As stated earlier, all answers can only be obtained through considerable interpretive efforts.

The scope of the overall scientific effort is illustrated in Figure 5. The local oceanic descriptions will be made by a bulk oceanic mixed layer model (the Garwood Model). The atmospheric descriptions will be made by the Naval Postgraduate School (NPS) Marine Atmospheric Boundary Layer model (Davidson et al 1983). Tactically significant

operational descriptions (forecasts) to which the improved understandings would apply, appear on the extreme right hand side of Figure 5.

B. MARINE ATMOSPHERIC BOUNDARY LAYER (MABL) MODEL

The NPS boundary layer model is a zero-order, two layer, integrated mixed layer model. The two layers consist of the well-mixed, turbulent boundary layer, and the relatively non-turbulent free atmosphere. The model is based on entrainment energetics formulated by Stage and Businger (1981) and on radiative transfers described by Davidson et al (1983).

The inversion (or transition zone) separates one layer from the other. In a zero-order model, the inversion is assumed to have zero thickness, hence, a discontinuity, or jump occurs in the profiles of the conservative parameters at the inversion.

The present model requires as input, an initial atmospheric sounding, the mean winds at a level within the surface layer (10-30 meters) and the surface temperature. Boundary layer wind values for the duration of the forecast period can be obtained from larger scale models. In this study, actual hourly wind speed measurements were input as

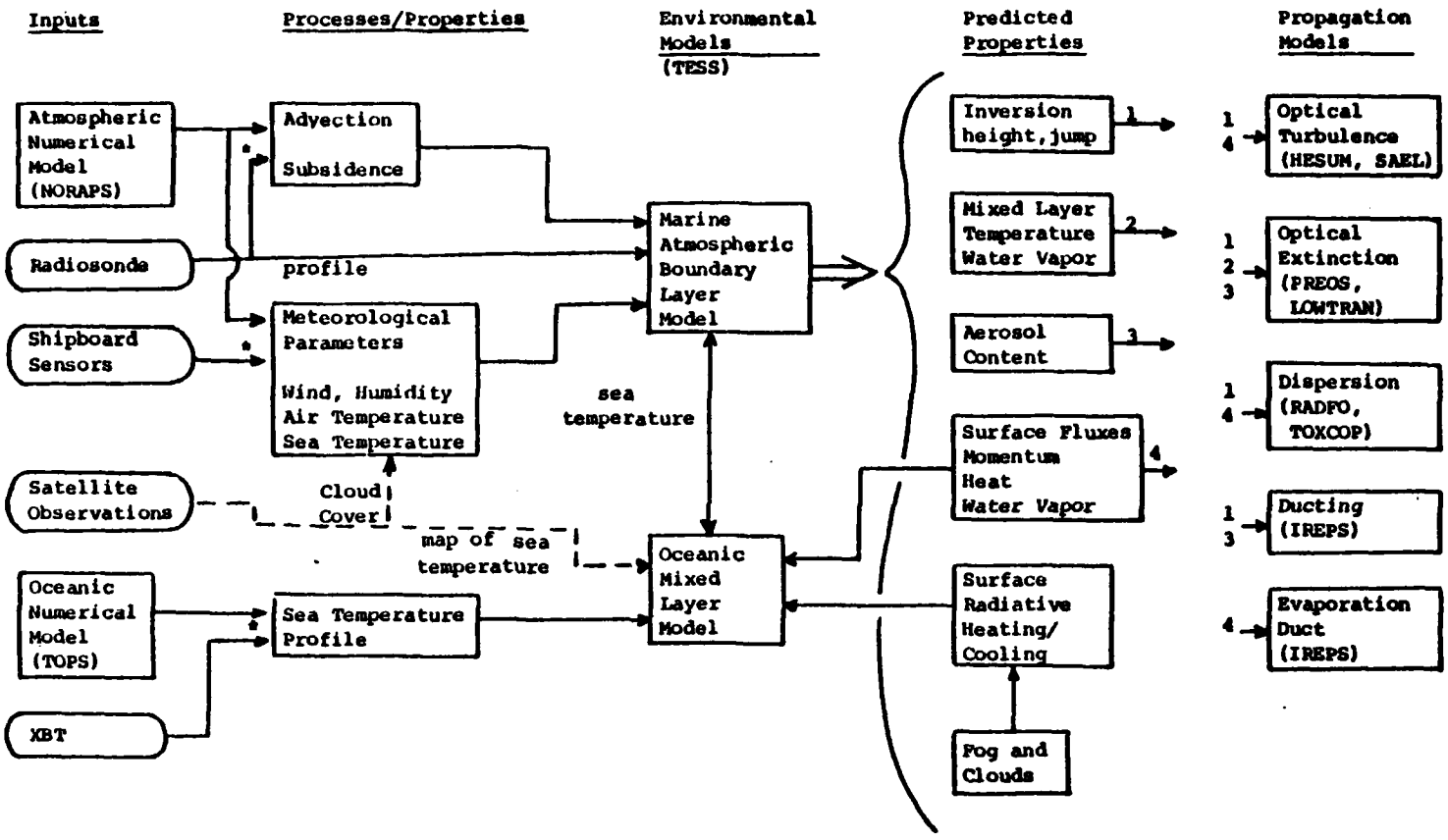

Figure 5. Simplified Flow Diagram of the Boundary Layer Model showing possible configurations of input information, interrelation between atmospheric and oceanic models, model outputs, and tactical models which use these outputs.

part of the model initialization. Sea-surface temperature remains unchanged from the initial input value. However, in the coupled model, the sea-surface temperature will change during the forecast period and will be that predicted by the OBL model. Well-mixed temperature and humidity are predicted so the surface wind and wind shear at the inversion are the only atmospheric variables which have to be prescribed. The larger scale subsidence, obtained from the large scale model must also be prescribed for the forecast period.

Three methods can be used to compute the large scale vertical velocity (subsidence) from single station observations. These three methods are well described by Gleason (1982) and include the kinematic and adiabatic methods and the integration of the moisture budget equation (Q-method). Gleason's study showed the Q-method displayed the most merit as a single-station assessment of subsidence. This method was used to compute subsidence for this study. The solar zenith angle used in the computation of the short wave radiative flux is determined from the latitude, julian day and time of day of the initial input.

The model predicts the time evolution of the inversion height, and the mixed layer values of θ (temperature) and q

(humidity), as well as their jumps, at 30-minute intervals. The prediction model is run out to 24 hours. The steps in the prediction computation are shown in Figure 6, where it is noted that procedures are the same for clear and cloudy cases except for entrainment computation and estimation of cloud top cooling.

The model uses the standard integrated rate equations (Tennekes and Dreidonks, 1981) to predict the time evolution of the conservative variables and their jumps at the inversion. These equations are:

$$h(Dx/Dt) = (w'x')_0 - (w'x')_h + \text{source} \quad (1)$$

$$h(D\Delta x/Dt) = h\Gamma x(\partial h/\partial t) - (w'x')_0 + (w'x')_h - \text{source} \quad (2)$$

where Γ is the lapse rate above the inversion and the source term is equal to $-(F_{nh} - F_{no})/\rho c_p$ for $x=\theta$ and equal to zero for $X=q$. F_n is the net radiative flux. The subscripts zero and h refer to surface and inversion height values, respectively.

Stage and Businger's (1981) entrainment velocity parameterization is used to close the system of equations and determine the time evolution of the inversion height. The closure assumption states that the dissipation rate of the

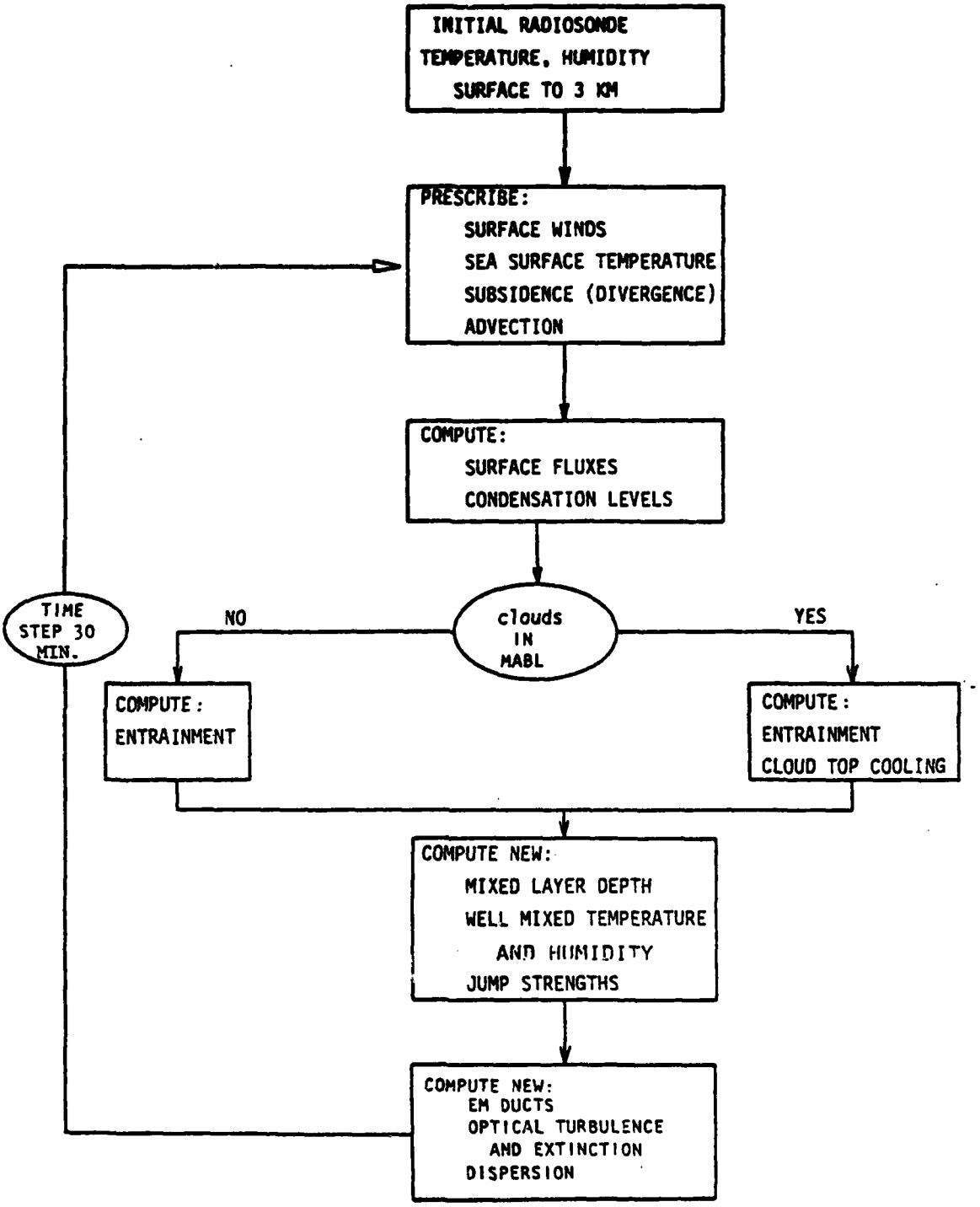

Figure 6. Schematic of Input, Prescription and Computing Steps in MABL Prediction.

turbulent kinetic energy (TKE) is a fraction (1-A) of the preduction rate. 'A' is the entrainment coefficient, taken as 0.2.

Mathematical modeling of radiative flux transfer is an extremely complicated but still developed subject. Unfortunately, even the simple radiative transfer models are still extremely complex in comparison to most other physical parameterizations used in the mixed layer model. Uncertainty in background aerosols, atmospheric absorbing gases (water vapor, carbon dioxide, ozone) and cloud droplet size spectra are sources of error in radiation calculations. Long and short wave radiation fluxes are computed separately.

The long wave radiation flux calculation was modified to permit non-black stratus clouds by introducing the cloud emissivity, ε_c, which is a function of the total cloud liquid content, W. Since the cloud liquid water profiles are approximately linear with height (Davidson et al, 1982), cloud liquid water content and cloud emissivity are given by:

$$W = 0.5 \rho_a (h - z_c) q_{lh} \tag{3}$$

$$\varepsilon_c = 1 - \exp(-aW) \tag{4}$$

where ρ_a is the density of air (1.25×10^{-3} gm cm^{-3}), h is the height of the mixed layer (cloud top), Z_c is the lifting condensation level (cloud bottom), a=0.158 (Slingo, 1982), and q_{lh} is the liquid water content at the cloud top.

The long wave cloud top net radiation flux, L_{nh}, can be calculated from the cloud top temperature, T_h, and the effective radiative sky temperature, T_{sky}, using the Stefan-Boltzmann Law. At the cloud bottom, this flux, L_{nc}, is calculated in the same manner using the sea surface temperature, T_s, and cloud bottom temperature, T_c. These fluxes are given by:

$$L_{nh} = \varepsilon_c \sigma (T_h^4 - T_{sky}^4) \qquad (5)$$

$$L_{nc} = \varepsilon_c \sigma (T_s^4 - T_c^4) \qquad (6)$$

where σ is Stefan's constant (4.61×10^{-11}) and ε_c, cloud emissivity, is obtained from equation 4. The net long wave flux at the surface, F_{long}, becomes:

$$F_{long} = \sigma (T_s^4 - \varepsilon_c \bar{T}^4 - (1-\varepsilon_c) T_{sky}^4) \qquad (7)$$

where $\bar{T}$ is the average temperature of the cloud. For the cloud free case, the net fluxes are calculated at Z=h and Z=0 using the standard method (Fleagle and Businger, 1978) of integrating the flux emissivity profile. The net long wave flux at the surface for the clear sky case is:

$$F_{long} = F_u - F_d \qquad (8)$$

where F_u is the upward radiative flux and F_d is the downward radiative flux.

Surface flux parameterization (bulk aerodynamical) formulae

$$u^* = C_d^{1/2} u_{10} \qquad (9a)$$

$$T^* = C_\theta^{1/2} (\theta_0 - \theta) \qquad (9b)$$

$$q^* = C_\theta^{1/2} (q_0 - q) \qquad (9c)$$

are used to determine the surface fluxes of momentum, sensible heat and latent heat. These fluxes are given by:

$$u'w' = u^{*2} \quad \text{(momentum)} \qquad (10a)$$

$$T'w' = u^*T^* \quad \text{(sensible heat)} \qquad (10b)$$

$$q'w' = u^*q^* \quad \text{(latent heat)} \qquad (10c)$$

where C_d and C_θ are the ten meter stability dependent drag coefficient, θ is the potential temperature, and q is the specific humidity. The subscript zero denotes the surface value.

The short wave radiative flux is calculated using the delta-Edington method (Joseph, 1976). This was added to the model to account for heating of the mixed layer by solar

radiation. Short wave extinction is dominated by scattering (as opposed to absorption). This scattered radiation forms a second short wave radiative component usually referred to as 'diffuse' solar radiation. Scattering in the mixed layer is due to atmospheric particles, cloud droplets in the cloudy case and sea-salt aerosols in the cloud-free case. This MABL model computes both the direct and diffuse radiative components to determine the total short wave radiation flux at the surface. An explanation of the delta-Edington method and all of the parameters, atmospheric factors, and equations involved is a very complex subject and is beyond the scope of this paper. An excellent review of this subject has been published by Fairall (1981). An important short wave radiative parameter that is prescribed in the ABL model is the fraction of reflected short wave radiation, Ag, from the sea surface. It is taken as 0.1.

C. OCEANIC BOUNDARY LAYER (OBL) MODEL

Garwood (1977) developed an ocean mixed layer model using the Navier-Stokes equation of motion with the geostrophic component eliminated, the continuity equation in incompressible water, the heat equation from the first law of thermodynamics, the conservation of salt equation, and a linearized equation of state.

Prediction of the rate of deepening (or retreat) of the mixed layer is dependent upon an understanding of the dynamics of the entrainment process. The turbulence of the overlying mixed layer provides the energy needed to destabilize and erode the underlying stable water mass (Garwood 1977). Therefore, the turbulent kinetic energy budget is the basis for the entrainment. This system is closed using a mean-turbulent-field modeling of the vertically integrated equations for the individual TKE components, plus the inclusion of the bulk buoyancy and momentum equations.

Seperate vertical and horizontal equations for TKE are used to better handle the mixing process. Buoyancy produced energy is somewhat more efficient than shear production as a source of energy for vertical mixing because of its unique effect on the vertical component of the turbulent velocity. The bucyancy equation is generated from the heat and salt equations together with an equation of state:

$$\bar{\rho} = \rho_0 \left[1 - \alpha(\tilde{\theta} - \theta_0) + \beta(\tilde{S} - S_0)\right] \tag{11}$$

and buoyancy is given by:

$$\tilde{b} = g(\rho_0 - \tilde{\rho})/\rho_0 \tag{12}$$

where θ is temperature, S is salinity, ρ density, g gravity, and the constants α and β are the expansion coefficients for heat and salt, respectively. The tilde represents the total instantaneous value and the subscript zero denotes an arbitrary, but representative, constant value. Using b instead of θ (temperature) for the definition of buoyancy allows this model to be applicable in situations where evaporation and precipitation contribute significantly to the surface buoyancy flux. Temperature is in most cases considered to be the dominating factor in the density profile. The relative importance of the salinity effect on the short term evolution of the density profile is generally not significant (Miller, 1976).

Temperature and salinity profiles, and for extended forecasts, the wind driven horizontal current profiles, are required as input for model initialization. These are used to compute the mixed layer depth. The Garwood OBL model defines the mixed layer depth, h , as the shallowest depth at which the observed density value, σ_t , is $0.02\sigma_t$ units greater than the observed surface density value.

Ocean environmental parameters that have to be prescribed include; the fraction of short wave radiation

absorbed in the top one meter of the ocean, the radiation extinction coefficient for determination of the downward turbulent heat flux, and the critical Richardson number for a stability adjustment at the bottom of the mixed layer.

The parameters required for surface boundary condition computations include wind speed and direction, cloud cover, sea surface temperature, air temperature (dry bulb), dew-point temperature, incident solar radiation, and the rate of evaporation (E) and precipitation (P).

The turbulent fluxes of latent heat, Q_e, and sensible heat, Q_h, are estimated using the bulk aerodynamic formulae:

$$Q_e = C_d (.98E_s - E_a) u_{10} \qquad (13a)$$

$$Q_h = C_d (T_s - T_a) u_{10} \qquad (13b)$$

and the net back radiation is estimated from the empirical equation (Husby and Seckel, 1975):

$$Q_b = 1.14X\ 10^{-7}(273.16+T_s)^4 (.39 - .5E_a^{1/2}) (1 - .6C^2) \qquad (13c)$$

where E_s is the saturated vapor pressure of the marine air (0.98 corrects for salt defects), E_a is the vapor pressure of air based on the dew-point temperature, T_a air temperature, T_s sea surface temperature, and C is the fractional cloud cover. The upward heat flux, Q_u, is then given as:

$$Q_u = Q_e + Q_h + Q_b \qquad (14)$$

The solar radiation, Q_s, is given by:

$$Q_s = (1 - a\alpha^b)(1 - .66C^3)Q_0 \qquad (15)$$

where Q_0 is the clear sky radiation given by (Seckel and Beauday, 1973):

$$Q_0 = A_0 + A_1 \cos \theta + B_1 \sin \theta + A_2 \cos 2\theta + B_2 \sin 2\theta \qquad (16)$$

The constants a and b are adopted from Tabata (1964) and the cubic cloud cover correction from Laevastu (1960). The variable is the mid-day elevation angle of the sun. The coefficients (A_0, A_1, ect.) were calculated by harmonic representation of the values predicted in the Smithsonian Meteorological Tables (list 1958) with

$$\theta = (2\pi/365)(t - 21) \qquad (17)$$

where t is the julian day of the year.

Not all of the incoming short wave radiation penetrates the ocean mixed layer. Approximately half (for open ocean) is absorbed within the first meter. The amount absorbed varies from region to region depending on the amount of absorbing particles such as phytoplankton and yellow substance. More radiation will be absorbed in coastal regions

than in the open ocean regions. This portion of absorbed short wave radiation is therefore considered to be part of the upward heat flux. The remainder of the short wave radiation does penetrate the mixed layer and is attenuated in an exponential fashion depending on water turbidity. If the fraction of solar radiation absorbed in the first meter, Rf, is given, then the net heat at the surface is given by:

$$Q_{net} = Q_u + (Rf)\,Q_s - Q_s \tag{18}$$

From these, the surface fluxes of buoyancy (heat and salt) and momentum can then be computed. The turbulent temperature, salinity, velocity and buoyancy fluxes are given by:

$$(T'w') = -Q_{net}/\rho c_p \tag{19a}$$

$$(S'w') = (P-E)\,S_0 \tag{19b}$$

$$(u'w') = u^{*2} \tag{19c}$$

$$(b'w') = g[\alpha(T'w') - \beta(S'w')] \tag{19d}$$

respectively, where u*, friction velocity in air, is calculated by:

$$\tau_s = \rho_a C_d u_{10}^2 \tag{20}$$

$$u^* = (\tau_s/\rho_a)^{1/2} \tag{21}$$

The subscript zero refers to the surface value and τ_s is the surface stress (dynes cm^{-2}). In this model, a positive buoyancy results when Qnet<0 and E>P. During daytime periods, negative buoyancy flux results from the domination of the solar heating at the surface, while during the night periods, a positive buoyancy flux is produced by the combined effect of net long wave radiation and the upward turbulent fluxes of heat and moisture.

New ocean temperature, salinity and wind driven current profiles are predicted at one hour intervals. These are then used to predict the new mixed layer depth. The steps in the prediction computation are shown in Figure 7.

D. FORMULATED COUPLED BOUNDARY LAYER MODEL

The physical processes described in the preceding two sections were not altered during the coupling steps. Some modifications were involved in transferring parameters between the models. Also necessary was the uniformity of units. The only parameter supplied from the ocean model for use in atmospheric computations is the predicted sea surface temperature. However, this prediction is influenced by many atmospheric parameters.

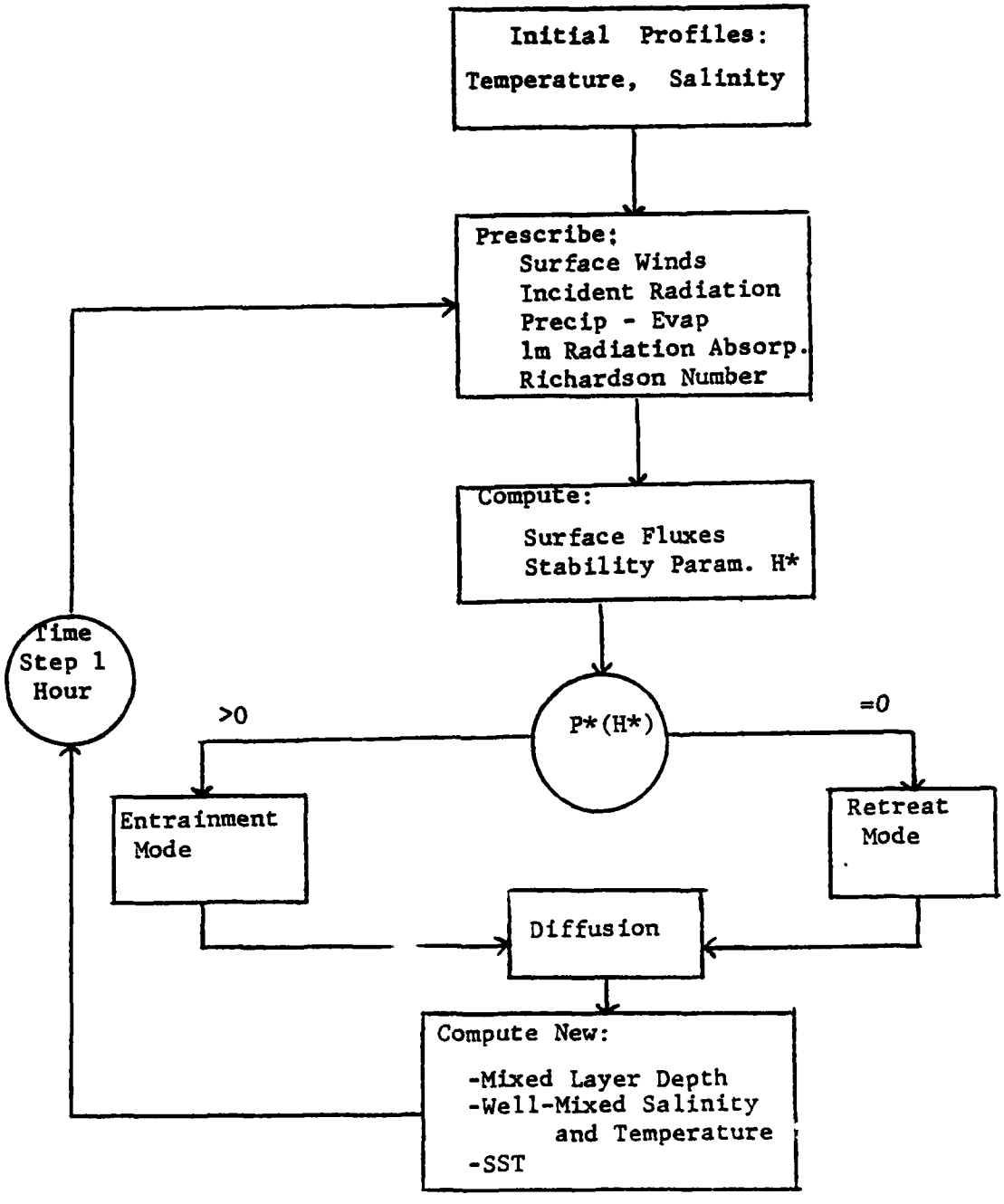

Figure 7. Schematic of Input, Prescription and Computing Steps in OBL Prediction.

Parameters in the atmosphere initialization include; wind speed and direction, dew-point temperature, latitude, julian day, and time of day. Short wave radiative flux (direct and diffuse), long wave radiative flux, sensible and latent heat fluxes, and the surface momentum flux were computed by the atmospheric section of the coupled model and input to the ocean model.

The first problem associated with the coupling involved the different prediction time steps of the seperate models. The atmospheric model uses a 30-minute time interval, whereas, the ocean model uses a one-hour time step interval. Assuming no significant sea-surface temperature change would take place over the short one-hour interval, the ocean model's prediction scheme was inserted into the atmosphere model as a subroutine. This prediction scheme is only called every other 30-minute time step. The ocean model's initialization routines are executed immediately upon the completion of the atmosphere model's initialization.

The second problem was with wind input. The ABL model does not require wind direction as an input parameter, only the magnitude of the wind speed. However, the ocean model requires wind direction to compute the horizontal components

of the winds. These components are used to determine the ocean turbulent velocity flux, u^{*2}_w, components used in the momentum budget computations. A new subroutine was added in the initialization scheme to determine the horizontal wind components from wind speed and direction input. These components are determined by:

$$u_{10x} = -(\sin \theta) u_{10} \tag{22a}$$

$$u_{10y} = -(\cos \theta) u_{10} \tag{22b}$$

where u_{10} is the specified wind speed at 10 meters and the east-west and north-south components are u_{10x} and u_{10y}, respectively. θ is the direction from which the winds are blowing relative to true north. Use of equations 20 and 21 and the following relationship:

$$\tau_s = \rho_a u^{*2} = \rho_w u^{*2}_w \tag{23}$$

allows the ocean turbulent velocity flux (u^{*2}_w) to be determined (assuming the density of seawater, ρ_w, to be approximated by 1) by first computing the wind stress from atmospheric parameters and then equating the ocean turbulent velocity flux to the computed wind stress value. The horizontal components of the turbulent velocity fluxes u^{*2}_{wx} and u^{*2}_{wy}, are then easily computed by:

$$u^{*2} = C_d u_{10}^2 = C_d (u_{10x}^2 + u_{10y}^2) \quad (24)$$

$$u^*_{wx}{}^2 = C_d u_{10x}^2 \quad (25a)$$

$$u^*_{wy}{}^2 = C_d u_{10y}^2 \quad (25b)$$

The atmospheric derived values are computed using the MKS unit system and had to be converted to the CGS system prior to any oceanic computations. This conversion is done at the start of each ocean prediction run.

As discussed in section B, the short wave radiative flux is calculated using the delta-Edington method. The long wave radiative, sensible heat and latent heat fluxes are computed using equations 10a, 10b and 10c, respectively. A unit conversion from Watts m to cal cm s is required on these values prior to use by ocean model. This conversion is again done at the start of the ocean prediction run. A flow diagram of the steps in the coupled model's prediction computation is shown in Figure 8.

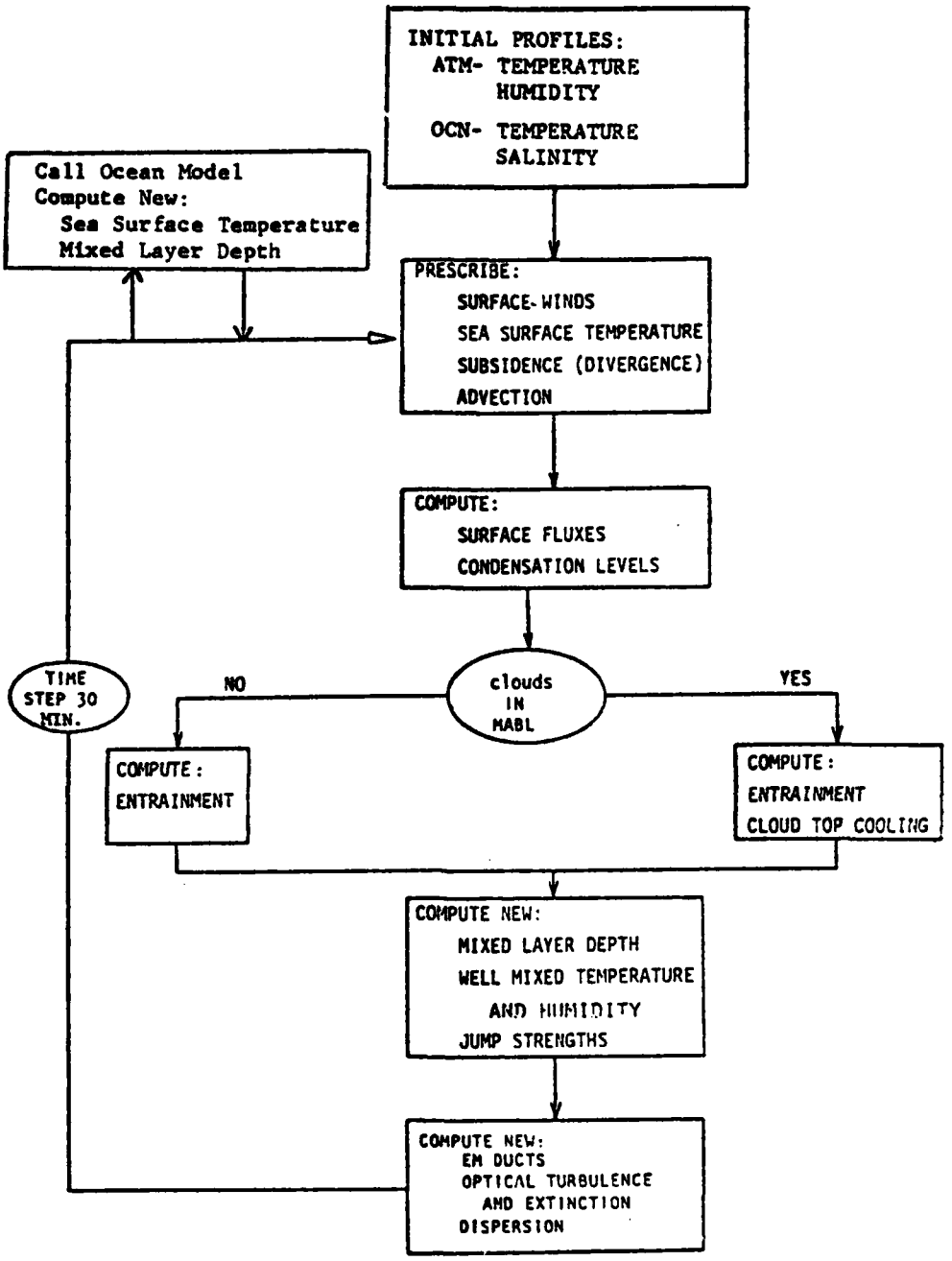

Figure 8. Schematic of Atmospheric and Oceanic Coupled Model. The ocean model is called at every other 30-minute time step to forecast prescribed surface temperature for the MABL prediction.

III. DATA AND MODEL RESULTS

The data sets used in this study are from the Cooperative Experiment on West Coast Oceanography and Meteorology from 21 September to 12 October 1976 (CEWCOM-76) and from 5 to 23 May 1978 (CEWCOM-78). Both were conducted in the Los Angeles-San Diego basin. Oceanic and atmospheric data were collected simultaneously throughout these time periods. XBT's were deployed from the R/V ACANIA on a regular basis (2-3 per day) in conjunction with atmosphere radiosondes. Sea surface temperature and atmospheric data such as winds, temperature, and relative humidity were also obtained continuously through these periods on board the R/V ACANIA.

Three 24-hour periods were selected for model initialization and verification. The first two cases cover a 48-hour period, 5/19/0500 to 5/21/0500 PST, during CEWCOM-78. This period coincides with the observations discussed in chapter 2, in which coupled air-sea interactions were cited as possible explanations for changes in both the atmospheric and oceanic mixed layer. Satellite imagery showed uniformly increasing stratus coverage (thin to heavy) during this 48-hour period. A clear sky situation was

chosen for the third case. This 24-hour period, 10/04/1900 to 10/05/1900 PST, was during CEWCOM-76.

The general location of the R/V ACANIA during these periods is shown in Figures 9, 10 and 11. During case 1 the ship was at anchor for the majority of the time period. The anchorage location is shown in Figure 9. For cases 2 and 3 the R/V ACANIA was cruising slowly (2-3 knots) returning to an initial point approximately every 12 hours. Winds were primarily from the west during the case 1 period. The winds shifted slightly to a west-northwest direction midway through the case 2 period. Winds for case 3 were primarily from the northwest and were much slower than in either case 1 or 2.

Two predictions were analyzed for each case, one prediction was based on the coupled air-sea boundary layer model, and the second prediction was with the atmospheric model with a fixed surface temperature. A separate oceanic prediction using fixed atmospheric parameters (persistence) was not made. This was the result of an initial modification that removed the wind stress and heat flux computation package in the ocean model in preparation for coupling with the atmosphere model.

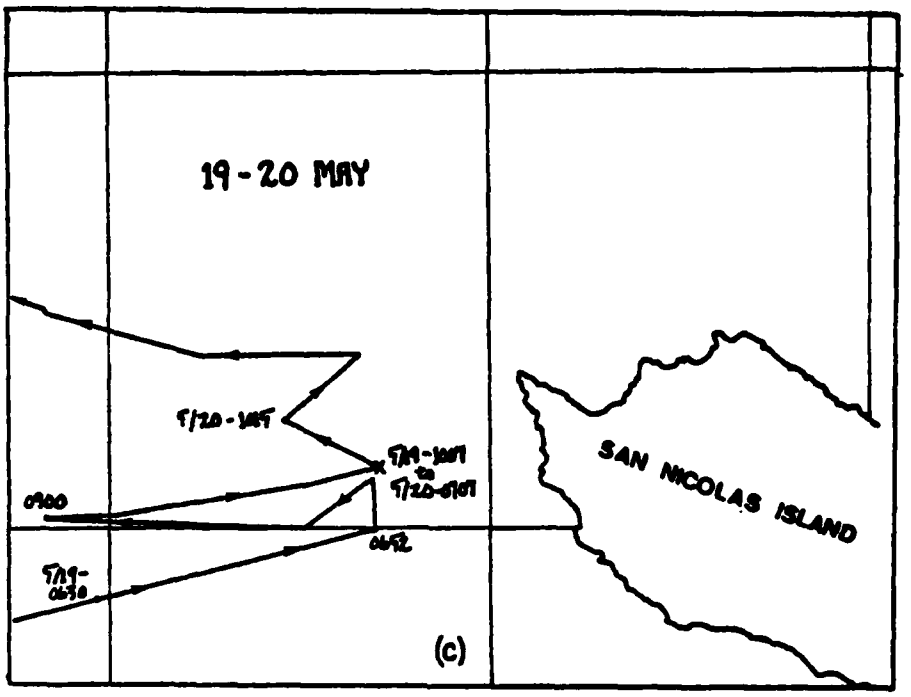

Figure 9. Anchorage Position of R/V ACANIA in the Vicinity of San Nicolas Island from 5/19/78 to 5/20/78.

Presentation of results will be in two parts. The first to be presented is the coupled model's performance with respect to observed oceanic and atmospheric variations. The second will deal with a comparison of predicted values between the coupled model and the atmospheric model. All tables and figures are grouped together by case number at the end of the chapter.

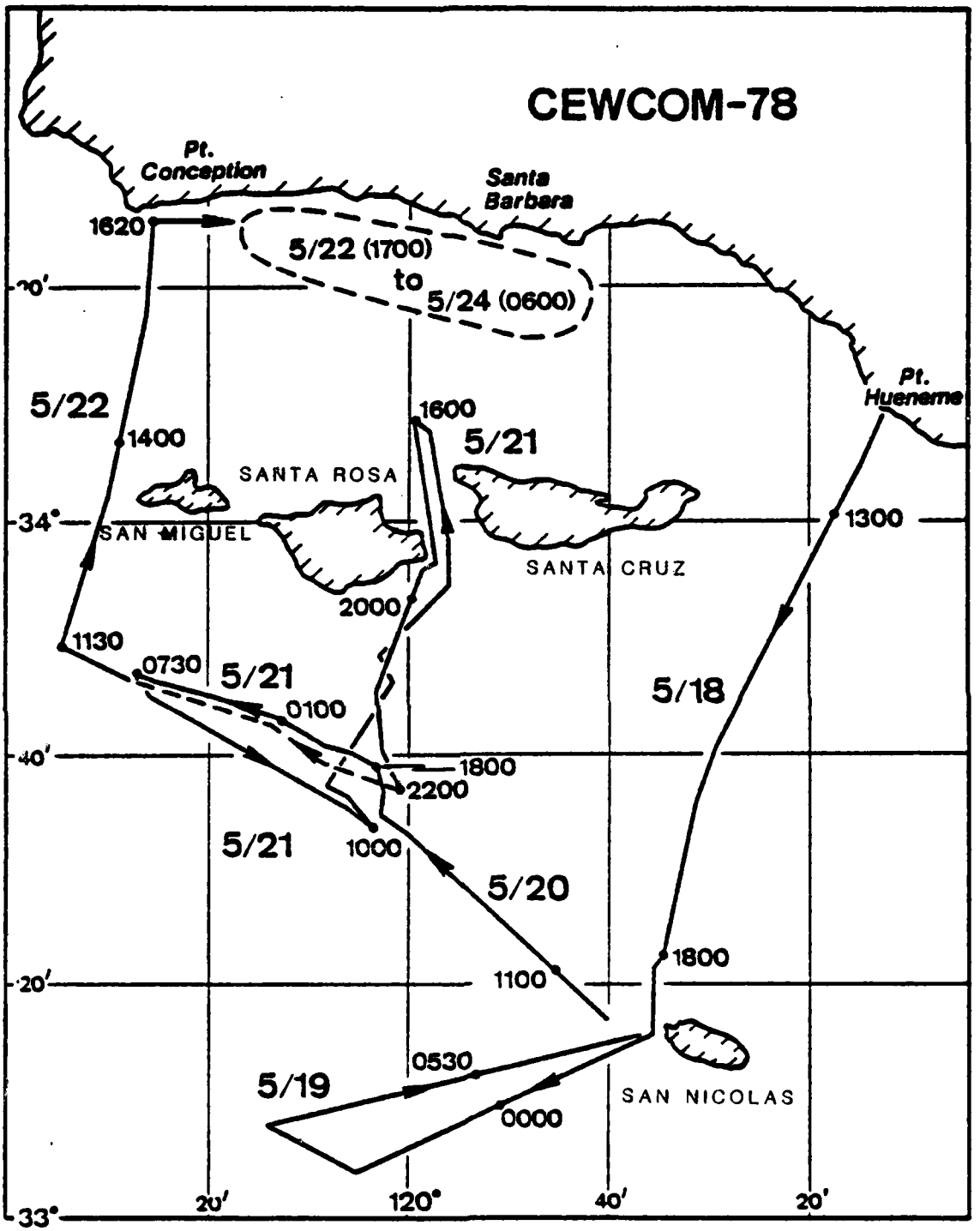

Figure 10. Positions of R/V ACANIA from 5/18/78 to 5/25/78.

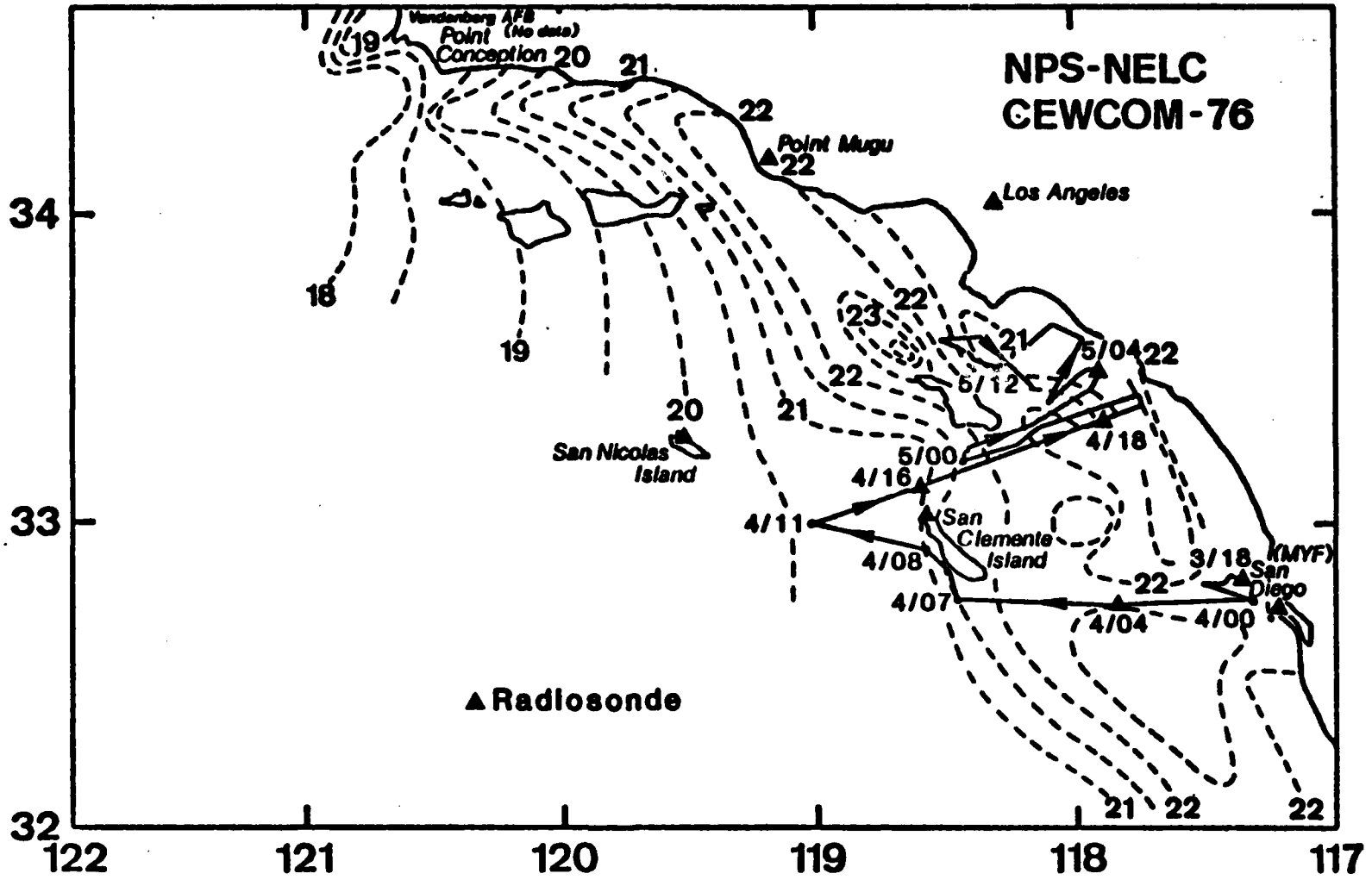

Figure 11. Positions of R/V ACANIA from 10/4/76 to 10/6/76. Horizontal temperature structure is shown by the dashed lines.

A. RESULTS FROM COUPLED MODEL

1. CASE 1 (0500 19 May to 0500 22 May)

A listing of predicted atmospheric and oceanic mixed layer quantities for this case appear in Table I. Values are for each 30-minute time step and since oceanic values are only computed at one-hour intervals, the same value appears at two time steps. The parameters listed include: height of inversion (Zi), height of lifting condensation level (Zlcl), wind speed (Wind), atmospheric mixed layer potential temperature (Th), evaporation duct height (Ze), sea surface temperature (SST), ocean mixed layer depth (MLD), and the net ocean surface heat flux (TW).

Predicted values are also shown in Figures 12 through 17. Figure 12 shows the time evolution of predicted sea-surface temperatures (solid line) and the values of the measured surface temperatures (dashed line). Figure 13 shows the time evolution of the ocean mixed layer depth. Figures 14-16 show ocean vertical profiles for temperature, u and v wind driven current velocities, and the salinity change from an initial value of 33.5 ppt, respectively. Figure 17 shows predictions of atmospheric parameters.

High solar insulation during the daytime results in a net downward heat flux (ocean warming). This can be readily observed in the net surface heat flux values (TW), in Table I, with the negative sign appearing during the daytime hours. Maximum heating of the ocean occurred between 1300 and 1400 local time. This same pattern, warming in the daytime hours, is also observed in the sea surface temperature values, Table I and Figure 12.

The winds appeared to be fairly constant, 8 ms^{-1}, between 0500 and 1100 on the nineteenth. Wind mixing coupled with convective cooling at the surface caused the mixed layer depth to deepen slightly from 19.5 to 20.9 m (Figure 13). This deepening and net heat loss at the surface caused the surface temperature to drop. As heating of the sea surface began to increase due to the increase of solar radiation, a shallow mixed layer of 14 meters formed.

The winds rapidly decreased from 8 to 5 ms^{-1} at 1200. This coincided with a near maximum value of radiative heating causing a shallow 7 meter mixed layer to form in less than 1 hour. As daytime heating continued, a shallower mixed layer of 3.5 meters formed. This process is referred to as the 'afternoon effect' in acoustic literature and is a

quite common phenomenon in many areas of the ocean. In Figure 14, the 7 meter mixed layer is barely discernible in the 1300 vertical temperature profile. The weak gradient at the base of the mixed layer only required weak mixed layer erosion (increase in winds or convective cooling) to break down the shallow mixed layer. During the late afternoon, the winds began to increase, and with the decreasing of solar radiation, the shallow thermocline was eroded away. The MLD continued deepening for the remainder of the time period due to wind-driven and convective mixing.

Since sea-surface temperature is the sole input from the ocean model to the atmosphere model, a comparison is made of predicted and actual sea-surface temperature values (Figure 12). Since the R/V ACANIA was at anchor during the majority of this time period, this is considered the best case to determine how well sea surface temperature changes due to atmospheric forcing are being predicted. The coupled model prediction yielded a 0.25°C temperature increase during the daytime heating period with a maximum temperature of 15.4°C at 1600 local time. A maximum surface temperature of 15.6°C was observed at 1600 giving a 0.2°C error.

After the daytime heating period, the surface temperatures began to drop. The minimum predicted surface temperature at the end of the 24-hour period was 15.2°C which yields a 0.2°C temperature drop. The 0.06°C temperature drop prior to ocean warming makes the magnitude of the predicted diurnal warming and cooling to be approximately equal. The actual minimum temperature at the end of the period was 14.96°C. Although there are small errors in the magnitude of the diurnal heating and cooling affects, the time evolution of this phenomenon is predicted quite well.

Precipitation was not observed during this period, therefore the surface moisture flux and surface salinity flux were due entirely to evaporation. The slight predicted increase in salinity from 33.5 to 33.5038 ppt, shown in Figure 16, is due to evaporation.

An unstable condition existed in the atmosphere during this prediction period. A strong buoyancy flux at the surface increases entrainment and should cause the inversion height to increase unless subsidence (associated with shallowing of the inversion height) is strong enough to prevent this increase. In this case, subsidence was relatively weak ($-.0028\ ms^{-1}$) and entrainment was able to increase the inversion height.

Cloud occurance/dissipation was of interest because of its effect on radiation at the surface. With the lifting condensation level, LCL, lower than the inversion throughout this time period, stratus clouds should be present during the entire period. This feature was observed. During this period the LCL decreased from 243 to 125 meters while the inversion height increased from 256 to 348 meters. This would indicate a thickening of the clouds over this 24-hour period which was also observed to be true. The air-sea coupling effect on predicting these cloud features cannot be identified until the results with a constant sea surface temperature forcing are examined. However, on the basis of the predicted temperature change, a significant influence by the coupling is not expected.

2. CASE 2 (0500 20 May to 0500 21 May)

A listing of predicted atmospheric and oceanic mixed layer quantities for this period are given in Table III and shown graphically in Figures 19 through 24. As in case 1, daytime heating at the surface is apparent by the negative signs in front of the net surface heat flux values. The maximum downward heat flux value was not as high as in case 1 and was probably due to thicker cloud conditions for this

case. However, increasing surface temperatures were observed during this heating period.

The winds increased steadily from 6 to 11 ms^{-1} throughout the first half of this period and slowly decreased to about 9.4 ms^{-1} at the end of the period. The higher winds should be associated with increased wind mixing of the ocean mixed layer. The increased winds caused the mixed layer depth to deepen at the end of this peiod. This also reduced the shallowing of the mixed layer during the afternoon radiative heating period. The shallowest mixed layer formed at 16 meters versus 3.5 meters in the previous case. In Figure 21, the 20 meter thermocline is seen to be very weak, and with the higher winds, the shallower afternoon mixed layer lasted only a couple of hours.

The effects of the diurnal heating and cooling periods caused a 0.1°C temperature increase and a 0.15°C temperature decrease, respectively. Both values are also smaller than those predicted in case 1. Reasons for the smaller predicted increase are: 1) thicker clouds reduced the amount of solar heating during the day, thereby reducing the diurnal temperature increase; 2) the higher winds increased the vertical mixing, causing cooler water below to be mixed into

the upper layer and also increased the latent heat loss due to evaporation. thus reducing the total net heat flux at the surface; and, 3) the larger air-sea temperature difference increased the sensible heat loss, which also reduced the net heat flux. The decrease in the downward solar radiative heating and increase in sensible and latent heat losses were somewhat balanced by the decrease in the long wave heat loss due to the presence of the clouds. This decrease in the long wave heat loss was also the primary reason for the slightly smaller value in the nighttime cooling period.

Comparisons of the predicted surface temperature values with the actual values (Figure 19), show a noticeable difference. This is probably due to the fact that at 0700 local time on 20 May, the R/V ACANIA began cruising slowly to the northwest. The regional horizontal temperature structure must be taken into account. The southern California coastal bathymetry and associated currents greatly influence the sea surface temperature structure. The California Current brings in colder water from the north as it heads south along the coast. Near Point Conception, the current begins to turn to the southwest away from the coast. Due to coastal bathymetry, Point Conception also provides

sheltering for the intrusion of warm water along the coast from the south by the Davidson Current. The eddies and meanders of cold and warm water make the sea surface temperature structure complex in the CEWCOM experiment areas. The surface temperature variation observed by the R/V ACANIA appears to be due to oceanographic features.

The 1°C temperature increase in the first two hours, when the ship began moving to the northwest, indicates that the ship's transit was through one of the small warm eddy features. Two reasons for this are 1) Radiative heating of the ocean did not even begin until after the observed surface temperature had already begun to rapidly decrease, and 2) the higher winds would tend to mix the surface waters with the cooler water from below, thus causing a decrease in temperature not an increase. The short time duration of this warm feature also suggests a transit through an anomaly. With the ship only cruising at 2-3 knots, the warm anomaly still only lasted less than 4 hours.

The ship turned on a northerly course at 1300 and the rapid temperature decrease stopped. It is reasonably safe to infer from the sudden change in the surface temperature trend (rapid decrease to slight increase) that the ship

is initially crossing the temperature gradient contours and then followed a parallel course with these contours. This would make oceanic conditions more compatible with those in case 1. Since the 0.4°C temperature increase during the daytime heating period compares favorably with the value observed while the ship was at anchor, the increase is therefore presumably due to the diurnal heating.

The ship turned back to a west-northwest course shortly after 1800 and the surface temperature immediately began to decrease 1.5°C in 4 hours. Two hours after the end of this period, 0700, the ship came about and paralleled its previous course but in the opposite direction. An examination of the observed sea surface temperatures shows a rapid increase comparable to the decrease while heading in the opposite direction. This further substantiates the observed large temperature changes are not due to atmospheric forcing, but rather to the ship's movement through an oceanographic eddy or front.

Unstable atmospheric conditions existed during this period as well. The 1.5°C drop in the air temperature and a much smaller drop in the ocean temperature (0.2°C) coupled with higher wind speeds resulted in a large surface buoyancy

flux. This resulted in a much higher predicted inversion height change due to entrainment. The slightly smaller subsidence rate was also a factor in the greater predicted increase of the inversion height.

The lifting condensation level fluctuates up and down unlike the steady decrease in height in case 1. However, the height of the LCL never increased above the initial height and so with the large increase in height of the inversion, thickening of the stratus cloud deck is predicted to continue during this period as well.

3. CASE 3 (1900 04 OCT to 1900 05 OCT)

A listing of predicted atmospheric and oceanic mixed layer quantities are given in Table V and shown graphically in Figures 26 through 31. Although the time period for this case is in October, there are still many features occuring that are similar to the first two cases in May. The primary differences in this case, other than being a cloud-free case, are 1) the air and surface temperature are much warmer and 2) a much higher value of subsidence was observed.

Daytime heating is apparent in predictions for the clear sky case, as expected. The magnitude of the net ocean surface heat flux is, however, smaller than the value for

the thin stratus deck condition in case 1. This is presumably due to the difference in seasonal heating rate and will not be considered part of the local coupling effects.

The winds in case 3 are much weaker than in the first two cases. With the light winds and high downward surface heat flux during the day, a much shallower mixed layer might be expected. The ocean mixed layer depth (MLD) values in Table V (also shown graphically in Figure 25) show that an ocean mixed layer of 1 meter suddenly forms in less than an hour after heating began at 0900. This shallow thermocline is much stronger than in either case 1 or 2, and persists throughout most of the day (Figure 28). As the winds slowly increased late in the afternoon, the shallow mixed layer deepens. Without winds to mix this shallow region, surface heating is much greater in this case. A 0.6°C surface temperature increase was predicted to occur.

As in case 2, the ship's movement played a major role in the large variations in observed surface temperature values. This prevented the verification of the predicted surface temperature increase during the daytime heating period. Figure 11 shows the complex horizontal temperature structure in the CEWCOM-76 experiment area for the first

week of October. From this figure, it is hard to explain the large 2.8°C temperature drop during the first half of the period as the ship appeared to be heading into warmer water. The rapid temperature increase, starting at 0900, is obviously due to the ship transiting into the warm eddy feature north of Santa Catalina Island (Figure 11).

Unstable atmospheric conditions are also present during this time period. The high subsidence caused the inversion to be forced downward to within 72 meters of the surface. The lifting condensation level decreases even more rapidly and finally becomes lower than the inversion at the last hour of the forecast period. This implies the formation of a low stratus cloud deck. From Figure 33, fog and stratus clouds were observed to form in the CEWCOM experiment area.

B. COMPARISON OF COUPLED AND ATMOSPHERIC MODEL

The second and final phase of this study is to compare the previous coupled air-sea boundary layer model results with the atmospheric model results using a constant sea surface temperature. This comparison is to determine if any differences existed between the atmospheric predictions, and if so, determine if these differences are due to coupled

interactions. A listing of the atmospheric model predictions of atmosphere mixed layer parameters for cases 1, 2 and 3 are found in Tables II, IV and VI, respectively. Graphical presentations of these results are shown in Figures 18, 25 and 32. All tables and figures are grouped together by case number at the end of this chapter.

The initial comparison reveals no significant difference in the two predicted sets of mixed layer parameters, indicating a negligible effect of coupled interactions on atmospheric predictions for this short time period. The predicted inversion heights are essentially identical in both sets of predictions for all three cases (maximum difference of 2 meters). This is also found to be true for humidity and even the evaporation duct height predictions. This observation is somewhat surprising since there are significant interactions between the surface fluxes (evaporation) and these parameters. The close proximity of these parameters to the ocean surface would also imply a more significant impact even with small changes in sea-surface temperatures.

The only parameter that seems to be clearly affected by the coupling is the lifting condensation level. However,

even for the cloudy conditions of cases 1 and 2, this shows only a slight deviation. A maximum difference of only 5 meters is observed between the predictions for these cases. In the clear sky case under warmer and more humid conditions, there is a 30 meter difference observed in the two LCL predictions. However this occurred as the atmosphere approach near neutral conditions. This may indicate the model's inability to make reliable forecasts under stable atmospheric conditions.

Since a comparison of predicted ocean parameters between a coupled and independent ocean model was not made, no conclusions on this topic can be made at this time. Although tentative results indicate no definite advantages using a coupled model for the atmospheric predictions, the reverse may very well be true for oceanic predictions.

IV. CONCLUSIONS/RECOMMENDATIONS

On the basis of a limited study of several 24-hour predictions, surface temperature variations are not large enough to require ocean mixed layer processes in short term atmospheric forecasts. Carefully selected data sets and considerable interpretive efforts are essential if general conclusions are to be drawn on the relative roles of dynamic processes in both boundary layers. Further studies are required to determine the model's ability to better handle forecasts at longer time scales. Further studies should also include sensitivity analyses to define situations for which air-sea interaction effects are greatest. Studies of oceanic sensitivity to atmospheric forcing are required to determine the impact it will have on acoustical forecasts.

The CEWCOM-76 and 78 data, although able to supply simultaneous and oceanic data, suffered in two major respects First, the complexity of the horizontal temperature structure with meanders of warm and cold eddy features had definite impacts on observed data. Second, data was collected while the R/V ACANIA was transiting through a complex

ocean temperature structure. Changes in observed conditions under these circumstances can and did mask the interaction processes of interest.

Although the primary results of this study indicate coupled air-sea models are probably not necessary for short term atmospheric forecasts, a coupled model still has advantages, especially if long term forecasts are to become possible. Such a model would not be the single one-dimensional one considered here. However, this model offers many potential benefits as a multi-purpose model with single station assessment and prediction capabilities in the absence of shore-based support. A sound velocity profile (SVP) prediction capability could be easily incorporated into this model. In conjunction with present prediction capabilities, a multi-purpose model would be available for a wide range of needs. Ocean mixed layer depth and SVP predictions can be used in predicting ASW sensor capabilities. Environmental effects on the performance of weapons and sensors that depend on electromagnetic and electro-optical wave propagation can be evaluated using the same model.

TABLE I

Coupled Model Predicted Atmospheric and Oceanic Mixed Layer Quantities- Case 1.

HOUR	Zi	Zlcl	WIND	Th	SST	MLD	TW	Ze
0430	256	243	0.0	13.3	15.2	0.0	0.0000	0.0
0500	252	216	8.0	13.4	15.2	19.5	0.0000	7.2
0530	250	174	8.0	13.3	15.2	20.1	.0067	6.9
0600	250	130	8.0	13.0	15.2	20.1	.0067	6.4
0630	252	116	8.0	12.9	15.1	20.4	.0028	6.0
0700	256	121	8.1	12.8	15.1	20.4	.0028	6.0
0730	259	127	8.1	12.9	15.1	20.7	.0011	6.1
0800	262	132	8.1	12.9	15.1	20.7	.0011	6.1
0830	265	136	8.1	12.9	15.1	20.8	-.0007	6.2
0900	267	139	8.1	12.9	15.1	20.8	-.0007	6.2
0930	270	142	8.1	12.9	15.2	20.9	-.0028	6.3
1000	272	145	8.2	13.0	15.2	20.9	-.0028	6.3
1030	274	148	8.2	13.0	15.2	16.4	-.0045	6.3
1100	276	151	8.2	13.0	15.2	16.4	-.0045	6.3
1130	278	153	6.6	13.1	15.2	14.1	-.0057	6.3
1200	279	153	5.0	13.0	15.2	14.1	-.0057	6.2
1230	280	153	5.1	13.0	15.2	7.2	-.0066	5.2
1300	281	153	5.3	12.9	15.3	7.2	-.0066	5.2
1330	282	153	5.4	12.8	15.3	3.6	-.0066	5.2
1400	283	153	5.6	12.8	15.3	3.6	-.0066	5.3
1430	284	152	5.8	12.8	15.4	5.1	-.0052	5.4
1500	285	150	5.9	12.7	15.4	5.1	-.0052	5.4
1530	286	148	6.1	12.7	15.4	6.5	-.0032	5.5
1600	288	145	6.3	12.6	15.4	6.5	-.0032	5.6
1630	289	142	7.0	12.6	15.4	8.3	-.0008	5.6
1700	291	138	7.8	12.5	15.4	8.3	-.0008	5.9
1730	293	134	7.7	12.5	15.3	12.0	.0014	6.1
1800	296	130	7.7	12.5	15.3	12.0	.0014	6.1
1830	299	127	7.6	12.4	15.3	14.8	.0029	6.1
1900	301	125	7.6	12.4	15.3	14.8	.0029	6.1
1930	304	125	7.5	12.4	15.3	17.0	.0034	6.1
2000	307	125	7.9	12.4	15.3	17.0	.0034	6.1
2030	310	127	8.3	12.4	15.3	18.7	.0034	6.2
2100	313	128	8.1	12.4	15.3	18.7	.0034	6.4
2130	316	129	7.9	12.3	15.3	20.6	.0038	6.3
2200	319	129	7.7	12.3	15.3	20.6	.0038	6.3
2230	322	129	7.5	12.3	15.3	21.1	.0036	6.3
2300	324	129	7.3	12.3	15.3	21.1	.0036	6.2
2330	327	129	7.0	12.3	15.3	21.3	.0035	6.1
0000	329	129	6.8	12.2	15.3	21.3	.0035	6.0
0030	331	128	6.5	12.2	15.3	21.5	.0033	6.0
0100	333	127	6.3	12.1	15.3	21.5	.0033	5.9
0130	335	127	6.1	12.1	15.3	21.6	.0032	5.9
0200	337	126	6.1	12.0	15.3	21.6	.0032	5.8
0230	339	125	6.1	12.0	15.3	21.7	.0031	5.9
0300	341	125	6.1	12.0	15.3	21.7	.0031	5.9
0330	343	125	6.2	11.9	15.3	21.9	.0032	5.9
0400	344	125	6.2	11.9	15.3	21.9	.0032	6.0
0430	346	125	6.2	11.9	15.3	22.0	.0033	6.0
0500	348	125	6.2	11.9	15.3	22.0	.0033	6.0

TABLE II

MABL Model Predicted Atmospheric Mixed Layer Quantities-Case 1.

HOUR	Zi	Zlcl	WIND	Th	SST	MLD	TW	Ze
0430	256	243	8.0	13.3	15.2	0.0	0.0000	0.0
0500	252	216	8.0	13.4	15.2	0.0	0.0000	7.2
0530	250	174	8.0	13.3	15.2	0.0	0.0000	6.9
0600	250	130	8.0	13.0	15.2	0.0	0.0000	6.4
0630	252	117	8.0	12.9	15.2	0.0	0.0000	6.0
0700	256	123	8.1	12.9	15.2	0.0	0.0000	5.9
0730	259	128	8.1	12.9	15.2	0.0	0.0000	6.0
0800	262	133	8.1	12.9	15.2	0.0	0.0000	6.1
0830	265	137	8.1	12.9	15.2	0.0	0.0000	6.2
0900	267	140	8.1	12.9	15.2	0.0	0.0000	6.2
0930	269	143	8.1	13.0	15.2	0.0	0.0000	6.3
1000	272	146	8.2	13.0	15.2	0.0	0.0000	6.3
1030	274	149	8.2	13.0	15.2	0.0	0.0000	6.3
1100	276	151	8.2	13.0	15.2	0.0	0.0000	6.3
1130	277	153	6.6	13.1	15.2	0.0	0.0000	6.3
1200	279	153	5.0	13.0	15.2	0.0	0.0000	6.3
1230	280	153	5.2	13.0	15.2	0.0	0.0000	6.3
1300	281	152	5.4	12.9	15.2	0.0	0.0000	6.3
1330	282	150	5.6	12.8	15.2	0.0	0.0000	6.4
1400	283	150	5.6	12.8	15.2	0.0	0.0000	6.5
1430	284	149	5.8	12.7	15.2	0.0	0.0000	6.5
1500	285	147	6.0	12.7	15.2	0.0	0.0000	6.6
1530	286	145	6.1	12.6	15.2	0.0	0.0000	6.6
1600	288	141	6.3	12.6	15.2	0.0	0.0000	6.7
1630	289	137	7.0	12.5	15.2	0.0	0.0000	6.8
1700	291	133	7.8	12.5	15.2	0.0	0.0000	6.8
1730	294	130	7.7	12.5	15.2	0.0	0.0000	6.8
1800	296	126	7.7	12.4	15.2	0.0	0.0000	6.8
1830	299	123	7.6	12.4	15.2	0.0	0.0000	6.8
1900	302	122	7.6	12.4	15.2	0.0	0.0000	6.8
1930	305	122	7.5	12.3	15.2	0.0	0.0000	6.1
2000	308	123	7.9	12.3	15.2	0.0	0.0000	6.1
2030	311	124	8.3	12.3	15.2	0.0	0.0000	6.3
2100	314	126	8.1	12.3	15.2	0.0	0.0000	6.4
2130	317	126	7.9	12.3	15.2	0.0	0.0000	6.4
2200	320	127	7.7	12.3	15.2	0.0	0.0000	6.3
2230	323	127	7.5	12.3	15.2	0.0	0.0000	6.3
2300	325	128	7.3	12.3	15.2	0.0	0.0000	6.3
2330	328	128	7.0	12.2	15.2	0.0	0.0000	6.2
0000	330	127	6.8	12.2	15.2	0.0	0.0000	6.1
0030	332	127	6.6	12.2	15.2	0.0	0.0000	6.0
0100	335	127	6.3	12.1	15.2	0.0	0.0000	5.9
0130	337	126	6.1	12.1	15.2	0.0	0.0000	5.9
0200	338	125	6.1	12.0	15.2	0.0	0.0000	5.9
0230	340	125	6.2	12.0	15.2	0.0	0.0000	5.9
0300	342	125	6.2	11.9	15.2	0.0	0.0000	5.9
0330	344	125	6.2	11.9	15.2	0.0	0.0000	6.0
0400	346	125	6.2	11.9	15.2	0.0	0.0000	6.0
0430	347	125	6.2	11.9	15.2	0.0	0.0000	6.0
0500	349	125	6.2	11.8	15.2	0.0	0.0000	6.0

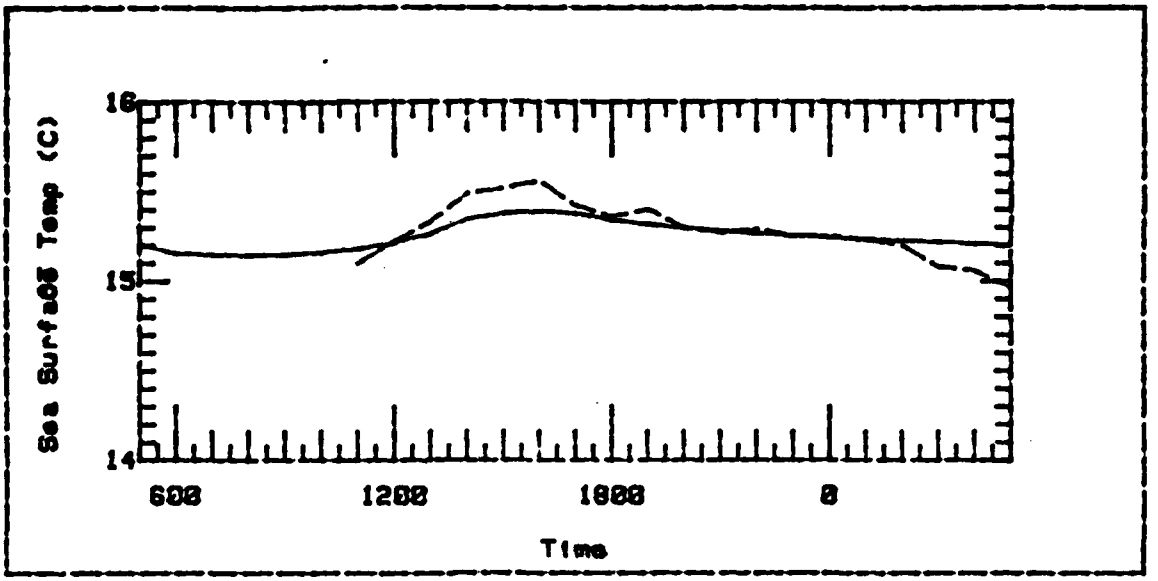

Figure 12. Time Evolution of the Sea-Surface Temperature-Case 1. Predicted values are shown by the solid line. Observed values are shown by the dashed line.

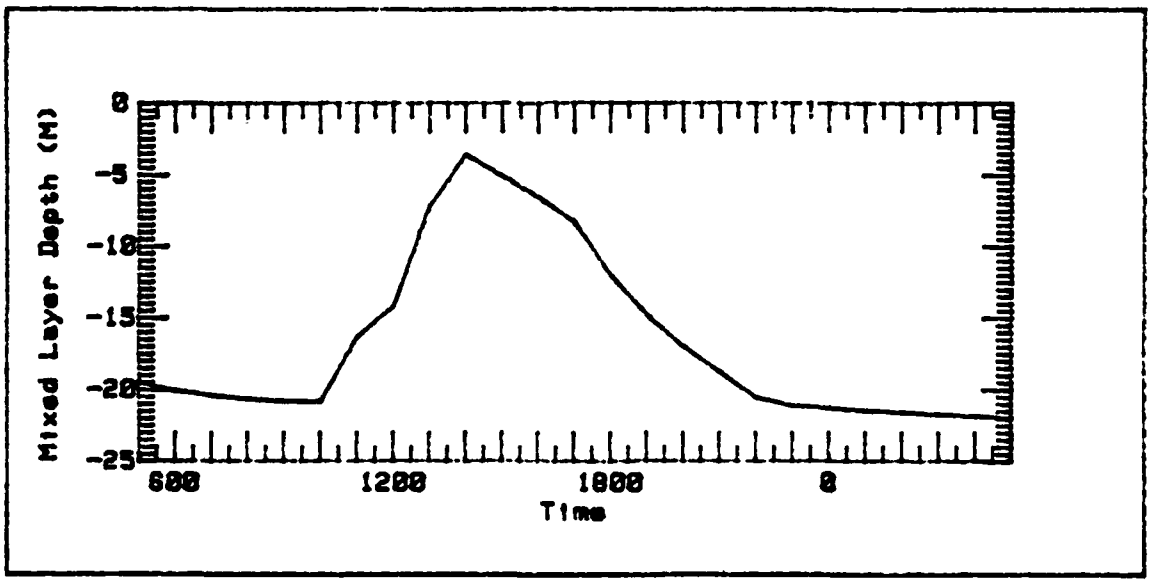

Figure 13. Time Evolution of Ocean Mixed Layer Depth (MLD)-Case 1.

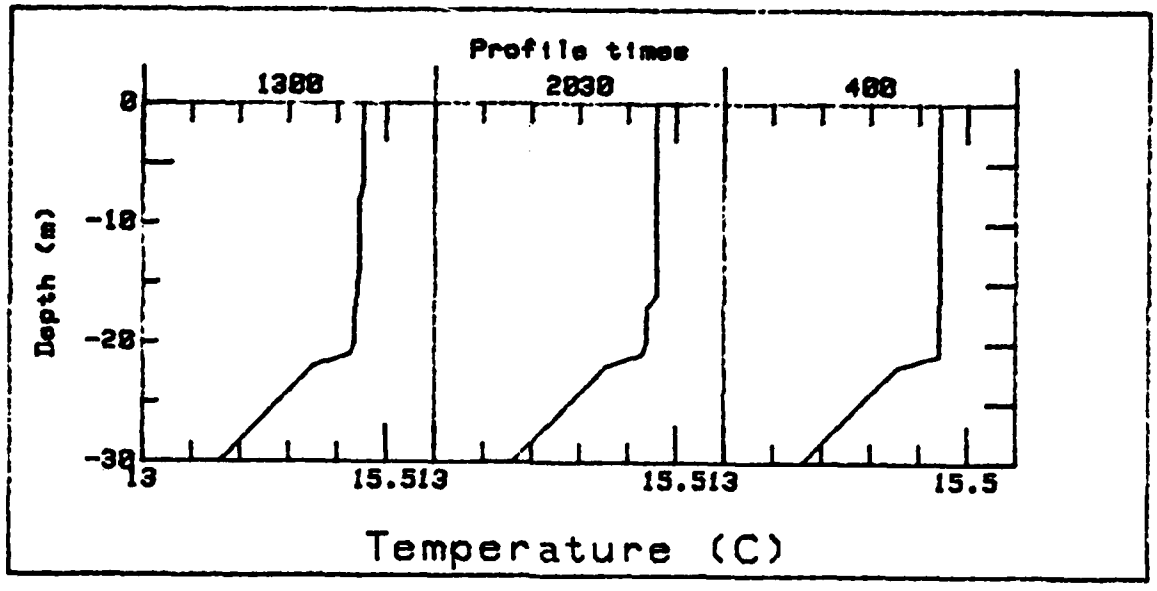

Figure 14. Selected Ocean Vertical Temperature Profiles- Case 1.

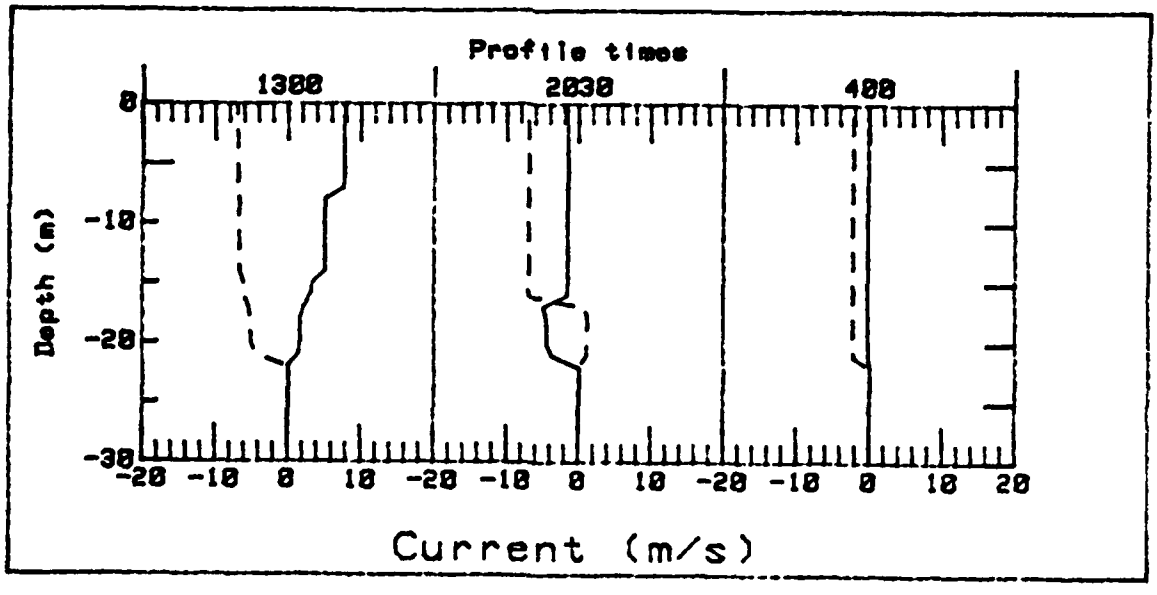

Figure 15. Selected Ocean Vertical Profiles of the Horizontal Wind Driven Currents- Case 1. East-west component u (solid line) North-south component v (dashed).

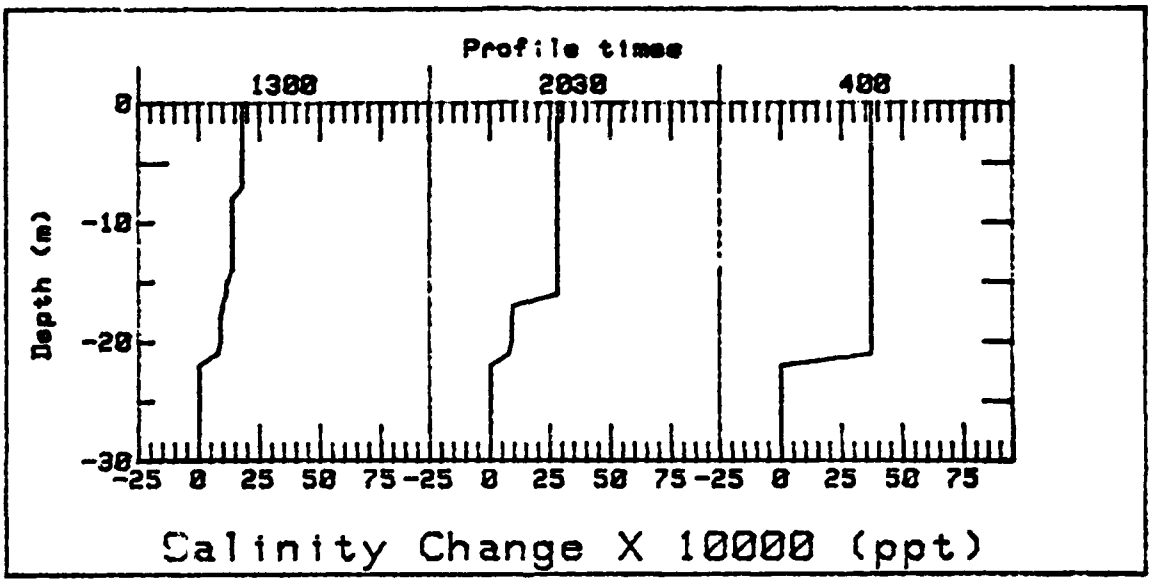

Figure 16. Selected Change in Ocean Vertical Salinity Profiles- Case 1.

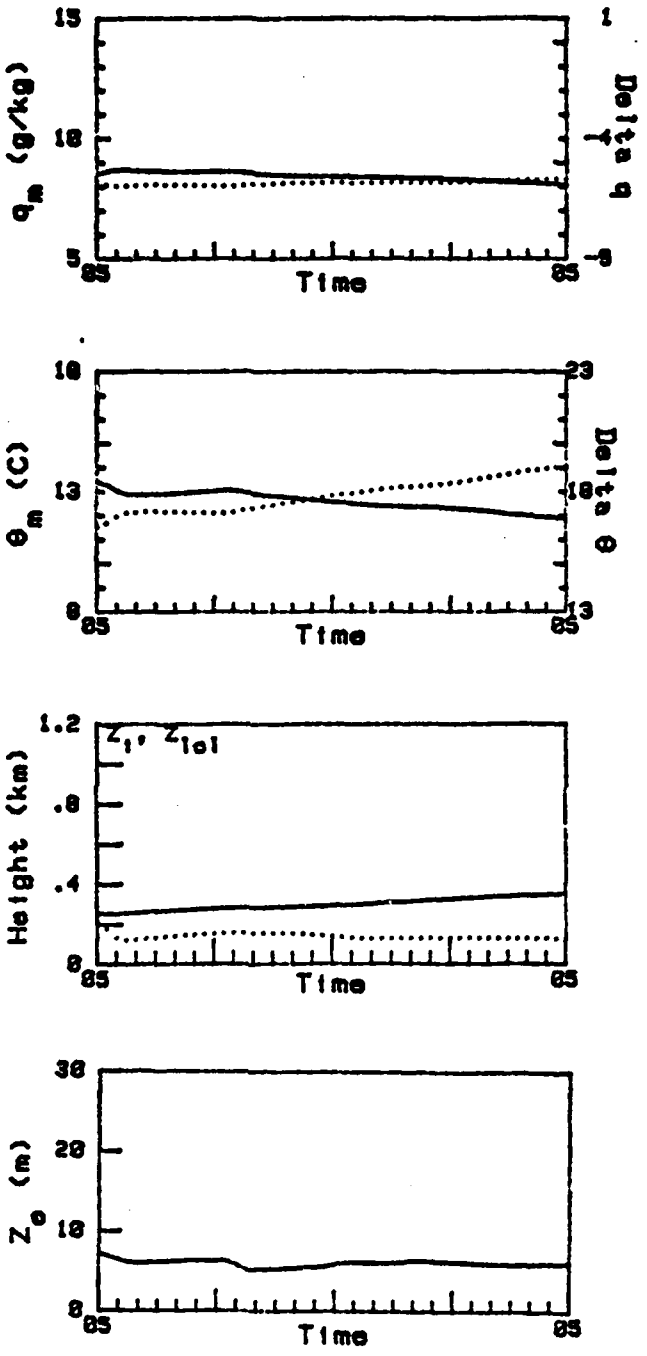

Figure 17. Graphical Display of the Coupled Model Predicted Atmospheric Mixed Layer Quantities- Case 1.

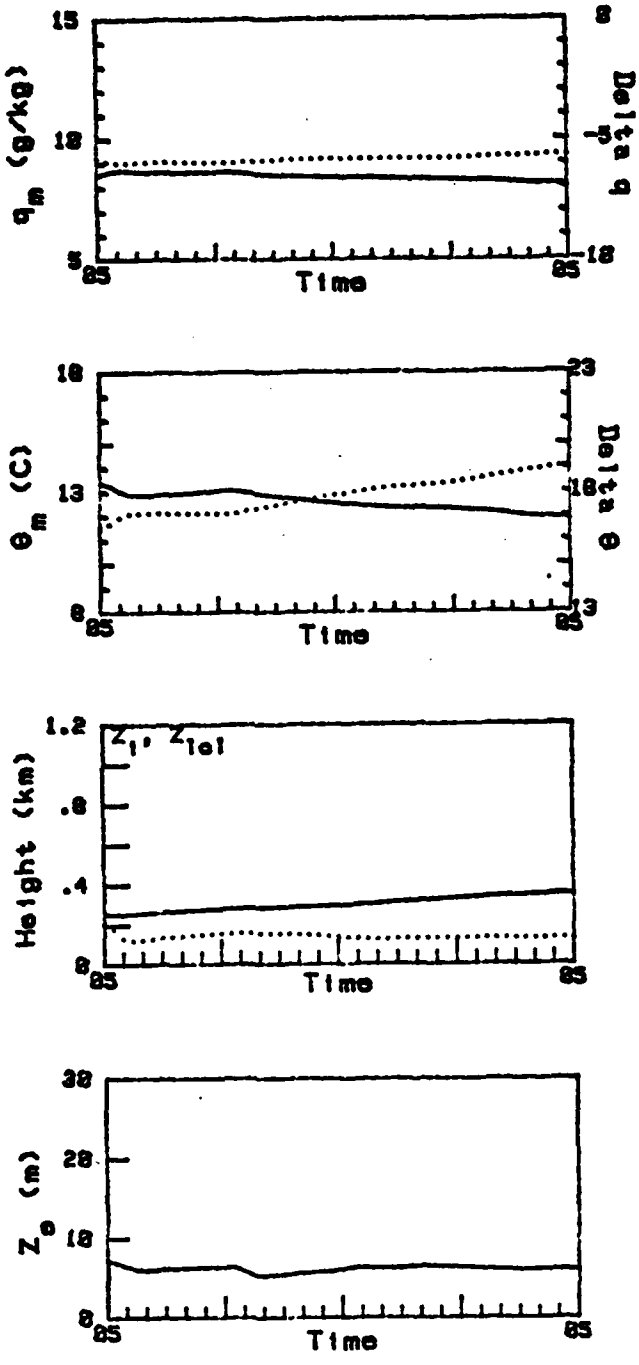

Figure 18. Graphical Display of the MABL Model Predicted Atmospheric Mixed Layer Quantities- Case 1.

TABLE I II

Coupled Model Predicted Atmospheric and Oceanic Mixed Layer Quantities- Case 2.

HOUR	Zi	Zlcl	WIND	Th	SST	MLD	TW	Ze
0430	351	316	0.0	12.0	15.0	0.0	0.0000	0.0
0500	350	284	6.4	12.0	15.0	0.5	0.0000	7.6
0530	351	249	6.4	11.8	14.9	0.7	.0055	7.3
0600	353	222	6.4	11.7	14.9	0.7	.0055	7.0
0630	357	208	6.4	11.7	14.9	0.8	.0032	6.8
0700	362	205	6.5	11.7	14.9	0.8	.0032	6.8
0730	368	209	6.7	11.7	14.9	0.8	.0019	6.8
0800	373	215	6.9	11.8	14.9	0.8	.0019	6.9
0830	378	222	7.2	11.9	14.9	0.9	.0004	7.0
0900	383	229	7.5	12.0	14.9	0.9	.0004	7.1
0930	388	235	7.8	12.1	14.9	0.9	-.0014	7.2
1000	393	242	8.2	12.3	14.9	0.9	-.0014	7.4
1030	399	248	8.5	12.3	15.0	1.1	-.0028	7.7
1100	403	254	8.3	12.4	15.0	1.1	-.0028	7.7
1130	408	260	8.2	12.5	15.0	0.0	-.0038	7.6
1200	413	264	8.1	12.6	15.0	0.0	-.0038	7.6
1230	417	268	8.1	12.7	15.0	16.8	-.0044	7.6
1300	421	272	8.3	12.7	15.0	16.8	-.0044	7.5
1330	425	275	8.5	12.8	15.0	17.3	-.0042	7.6
1400	430	277	8.7	12.9	15.0	17.3	-.0042	7.6
1430	434	278	8.9	12.9	15.0	18.7	-.0030	7.7
1500	438	279	9.0	13.0	15.0	18.7	-.0030	7.7
1530	443	279	9.2	13.0	15.0	20.5	-.0013	7.8
1600	448	278	9.4	13.0	15.0	20.5	-.0013	7.9
1630	453	276	9.6	13.0	15.0	4.4	.0007	7.9
1700	458	274	9.8	13.0	15.0	4.4	.0007	7.9
1730	464	271	10.0	13.0	15.0	4.1	.0024	7.9
1800	470	268	10.2	13.0	15.0	4.1	.0024	8.0
1830	477	267	10.5	13.0	15.0	4.3	.0037	8.0
1900	483	267	11.0	13.0	15.0	4.3	.0037	8.1
1930	491	268	10.9	13.0	15.0	4.6	.0044	8.0
2000	498	271	10.8	13.0	15.0	4.6	.0044	8.0
2030	505	273	10.7	13.0	15.0	4.9	.0045	8.0
2100	512	276	10.6	13.0	15.0	4.9	.0045	8.0
2130	519	278	10.5	13.0	15.0	4.2	.0044	8.0
2200	526	281	10.4	13.1	15.0	4.2	.0044	8.0
2230	533	283	10.4	13.1	15.0	4.4	.0043	8.0
2300	539	285	10.3	13.1	15.0	4.4	.0043	8.0
2330	545	287	10.2	13.1	14.9	4.7	.0043	8.0
0000	552	289	10.1	13.1	14.9	4.9	.0042	8.0
0030	558	291	10.0	13.1	14.9	4.9	.0042	8.0
0100	564	293	9.9	13.1	14.9	5.1	.0041	8.0
0130	570	295	9.8	13.1	14.9	5.1	.0041	8.0
0200	576	296	9.8	13.1	14.9	5.3	.0041	8.0
0230	581	298	9.8	13.1	14.9	5.3	.0041	8.0
0300	587	299	9.8	13.1	14.9	5.4	.0039	8.0
0330	592	300	8.8	13.1	14.9	5.4	.0039	8.0
0400	597	301	9.6	13.1	14.9	5.5	.0038	8.0
0430	601	302	9.8	13.1	14.9	5.5	.0038	8.0
0500	606	303	9.4	13.0	14.9	5.5	.0038	8.0

TABLE IV

MABL Model Predicted Atmospheric Mixed Layer Quantities-Case 2.

HOUR	Zi	Zlcl	WIND	Th	SST	MLD	TW	Ze
0430	351	316	0.0	12.0	15.0	0.0	0.0000	0.0
0500	350	284	6.4	12.0	15.0	0.0	0.0000	7.6
0530	351	249	6.6	11.8	15.0	0.0	0.0000	7.3
0600	353	222	6.7	11.7	15.0	0.0	0.0000	7.1
0630	358	209	6.9	11.7	15.0	0.0	0.0000	7.0
0700	363	206	7.0	11.7	15.0	0.0	0.0000	6.9
0730	368	210	7.2	11.8	15.0	0.0	0.0000	7.0
0800	374	217	7.3	11.9	15.0	0.0	0.0000	7.1
0830	379	224	7.5	12.0	15.0	0.0	0.0000	7.0
0900	385	231	7.6	12.1	15.0	0.0	0.0000	7.2
0930	390	238	7.8	12.2	15.0	0.0	0.0000	7.3
1000	395	244	8.7	12.2	15.0	0.0	0.0000	7.3
1030	400	250	8.6	12.4	15.0	0.0	0.0000	7.7
1100	405	256	8.5	12.5	15.0	0.0	0.0000	7.7
1130	409	261	8.3	12.6	15.0	0.0	0.0000	7.7
1200	414	266	8.2	12.6	15.0	0.0	0.0000	7.6
1230	418	270	8.1	12.7	15.0	0.0	0.0000	7.6
1300	423	273	8.3	12.8	15.0	0.0	0.0000	7.6
1330	427	275	8.4	12.8	15.0	0.0	0.0000	7.6
1400	431	277	8.6	12.9	15.0	0.0	0.0000	7.7
1430	436	278	8.7	12.9	15.0	0.0	0.0000	7.8
1500	440	279	8.9	13.0	15.0	0.0	0.0000	7.8
1530	445	278	9.1	13.0	15.0	0.0	0.0000	7.8
1600	450	277	9.3	13.0	15.0	0.0	0.0000	8.0
1630	455	275	9.5	13.0	15.0	0.0	0.0000	8.0
1700	460	273	9.6	13.0	15.0	0.0	0.0000	8.0
1730	466	270	9.8	13.0	15.0	0.0	0.0000	8.0
1800	472	267	10.0	13.0	15.0	0.0	0.0000	8.0
1830	479	266	10.5	12.9	15.0	0.0	0.0000	8.0
1900	486	266	11.0	13.0	15.0	0.0	0.0000	8.1
1930	493	268	10.9	13.0	15.0	0.0	0.0000	8.1
2000	500	270	10.8	13.0	15.0	0.0	0.0000	8.1
2030	507	273	10.7	13.0	15.0	0.0	0.0000	8.1
2100	514	276	10.6	13.0	15.0	0.0	0.0000	8.1
2130	521	278	10.5	13.0	15.0	0.0	0.0000	8.1
2200	528	281	10.4	13.1	15.0	0.0	0.0000	8.1
2230	535	284	10.4	13.1	15.0	0.0	0.0000	8.1
2300	541	286	10.3	13.1	15.0	0.0	0.0000	8.1
2330	548	288	10.2	13.1	15.0	0.0	0.0000	8.1
0000	554	290	10.1	13.1	15.0	0.0	0.0000	8.1
0030	560	292	10.0	13.1	15.0	0.0	0.0000	8.1
0100	567	294	9.9	13.1	15.0	0.0	0.0000	8.1
0130	572	296	9.8	13.1	15.0	0.0	0.0000	8.1
0200	578	298	9.6	13.1	15.0	0.0	0.0000	8.1
0230	584	300	9.3	13.1	15.0	0.0	0.0000	8.1
0300	589	301	9.1	13.1	15.0	0.0	0.0000	8.1
0330	594	303	8.8	13.1	15.0	0.0	0.0000	8.1
0400	599	304	8.6	13.1	15.0	0.0	0.0000	8.1
0430	604	305	9.0	13.1	15.0	0.0	0.0000	8.1
0500	608	306	9.4	13.1	15.0	0.0	0.0000	8.2

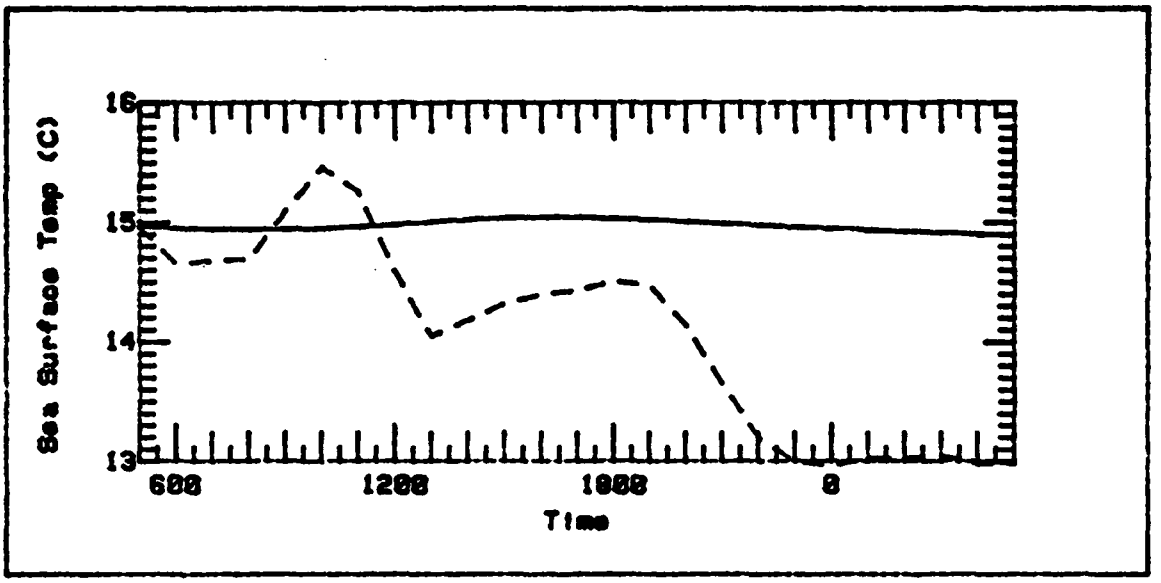

Figure 19. Time Evolution of the Sea-Surface Temperature-Case 2. Predicted values are shown by the solid line. Observed values are shown by the dashed line.

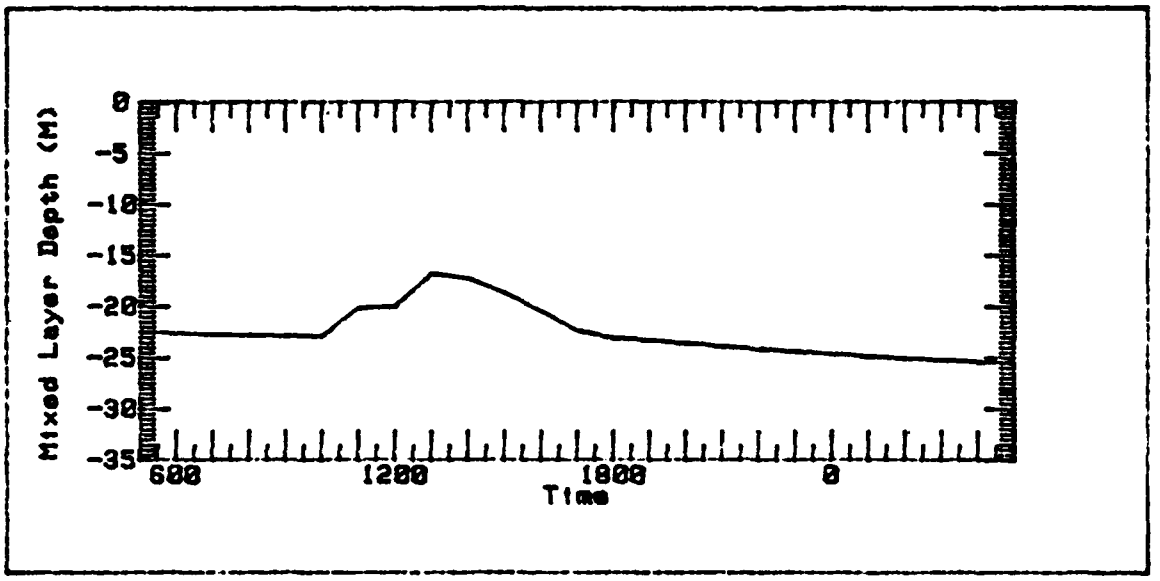

Figure 20. Time Evolution of Ocean Mixed Layer Depth (MLD)-Case 2.

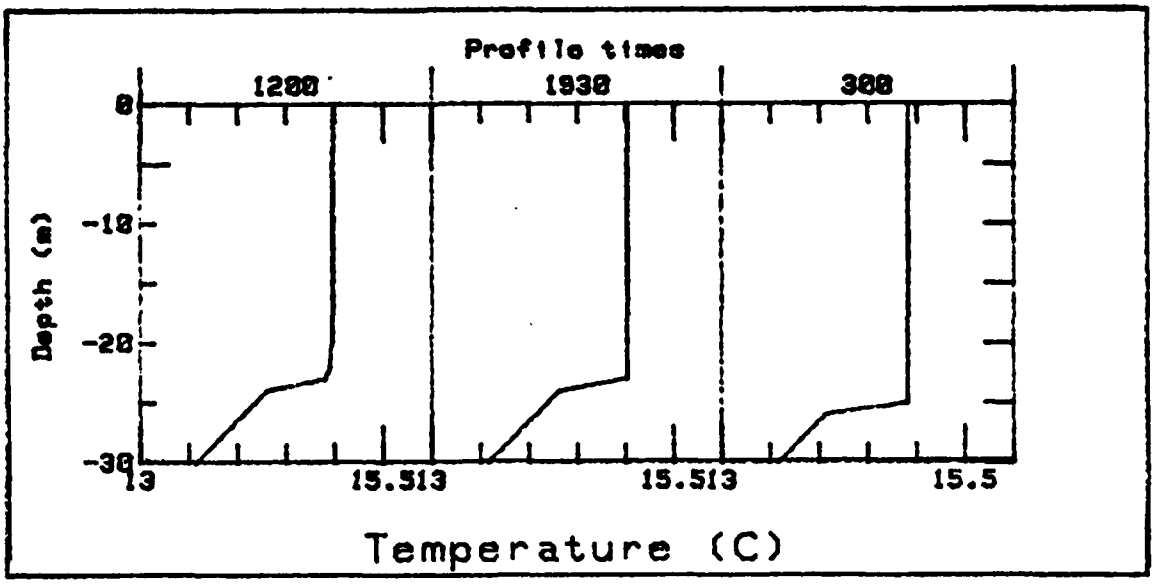

Figure 21. Selected Ocean Vertical Temperature Profiles- Case 2.

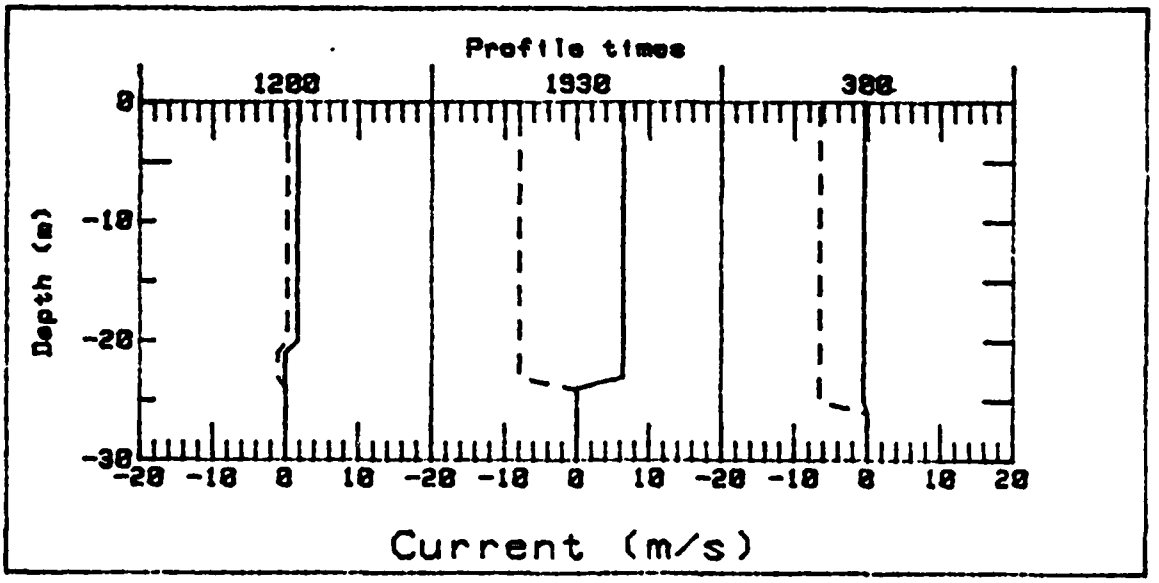

Figure 22. Selected Ocean Vertical Profiles of the Horizontal Wind Driven Currents- Case 2. East-west component u (solid line) North-south component v (dashed).

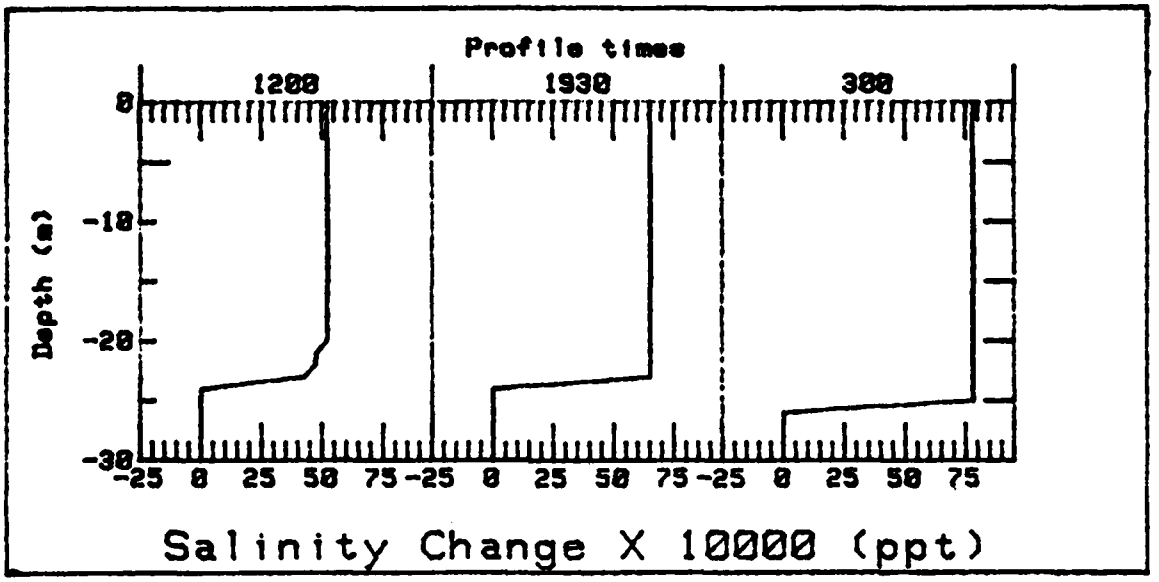

Figure 23. Selected Change in Ocean Vertical Salinity Profiles- Case 2.

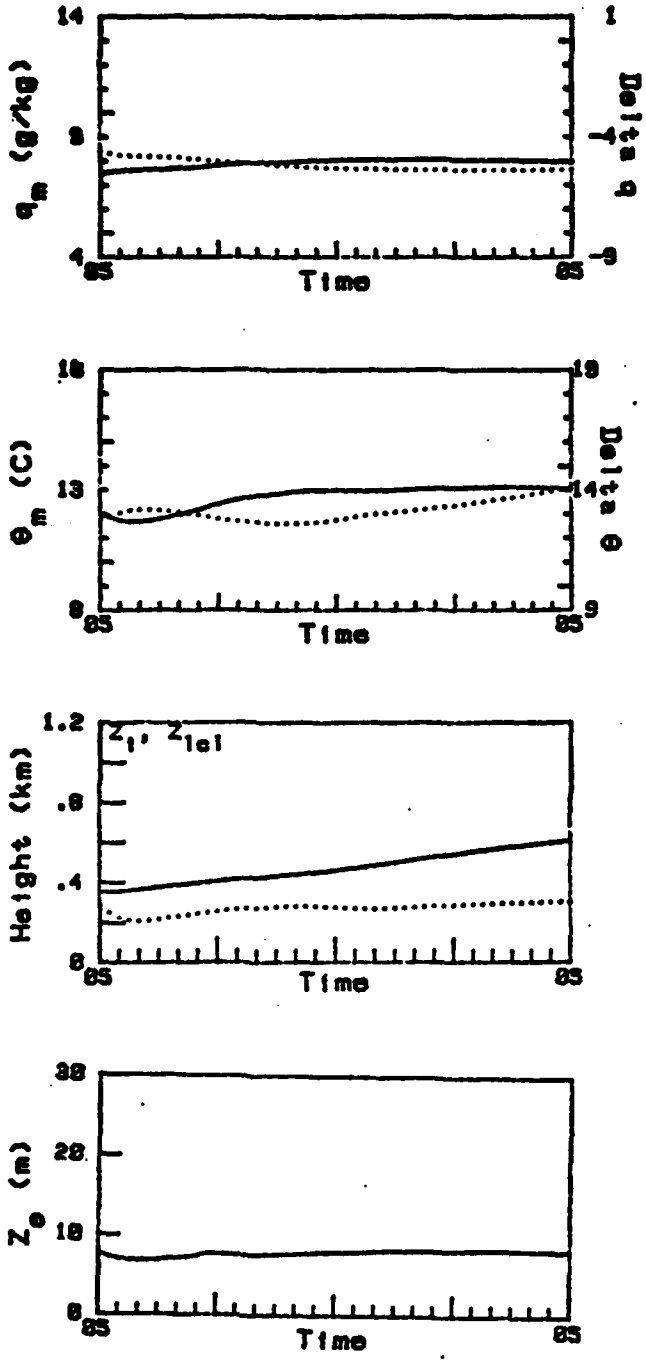

Figure 24. Graphical Display of the Coupled Model Predicted Atmospheric Mixed Layer Quantities- Case 2.

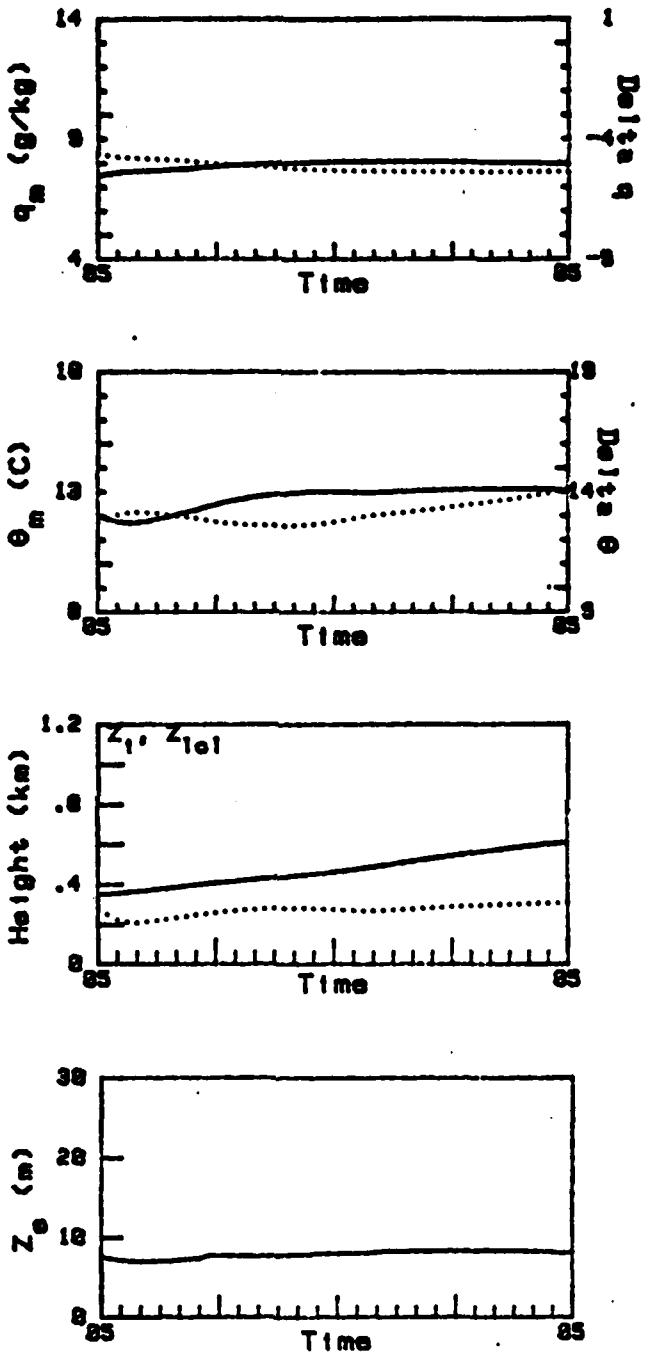

Figure 25. Graphical Display of the MABL Model Predicted Atmospheric Mixed Layer Quantities- Case 2.

TABLE V

Coupled Model Predicted Atmospheric and Oceanic Mixed Layer Quantities- Case 3.

HOUR	Zi	Zlcl	WIND	Th	SST	MLD	TW	Ze
1830	248	333	0.0	19.0	21.2	0.0	0.0000	0.0
1900	242	328	4.3	19.2	21.2	8.5	0.0000	8.1
1930	237	324	4.5	19.3	21.1	9.0	.0070	8.1
2000	232	319	4.7	19.5	21.1	9.0	.0070	8.3
2030	227	314	4.9	19.6	21.1	9.6	.0068	8.4
2100	222	307	5.1	19.8	21.1	9.6	.0068	8.6
2130	217	300	5.3	19.9	21.0	10.3	.0067	8.8
2200	212	292	5.5	20.0	21.0	10.3	.0067	8.9
2230	208	284	4.9	20.1	21.0	11.1	.0066	8.9
2300	203	276	4.4	20.2	21.0	11.1	.0066	8.4
2330	198	269	3.9	20.3	21.0	11.8	.0062	7.9
0000	193	263	3.5	20.4	21.0	11.8	.0062	7.4
0030	189	258	3.0	20.5	20.9	12.4	.0058	7.0
0100	184	252	3.0	20.5	20.9	12.4	.0058	6.7
0130	179	246	3.0	20.5	20.9	13.1	.0054	6.5
0200	175	240	3.4	20.6	20.9	13.1	.0054	6.4
0230	170	236	3.1	20.6	20.9	13.6	.0053	5.8
0300	165	231	3.1	20.6	20.9	13.6	.0053	5.3
0330	161	226	2.5	20.6	20.9	14.2	.0050	5.3
0400	157	220	2.6	20.7	20.9	14.8	.0050	5.8
0430	153	214	2.7	20.7	20.9	14.8	.0051	5.8
0500	149	207	2.9	20.7	20.9	14.8	.0051	5.9
0530	145	199	3.0	20.7	20.9	15.3	.0051	5.9
0600	141	191	2.7	20.7	20.9	15.3	.0051	6.0
0630	137	185	2.5	20.8	20.8	15.9	.0051	5.6
0700	133	182	2.2	20.8	20.8	15.9	.0051	5.4
0730	130	179	2.0	20.8	20.8	16.3	.0037	5.1
0800	126	177	1.7	20.9	20.8	16.3	.0037	5.0
0830	123	175	1.5	20.9	20.8	16.3	.0011	4.8
0900	119	172	1.0	20.9	20.8	16.3	.0011	4.6
0930	116	171	.5	20.9	20.9	1.0	-.0012	4.1
1000	112	171	1.4	21.0	20.9	1.0	-.0012	2.9
1030	109	169	2.3	21.0	21.0	1.0	-.0032	4.4
1100	106	166	2.4	21.0	21.0	1.0	-.0032	4.8
1130	103	163	2.7	21.1	21.2	1.0	-.0045	4.9
1200	101	162	3.1	21.1	21.2	1.0	-.0045	4.6
1230	98	160	3.7	21.2	21.3	1.0	-.0049	4.8
1300	96	164	4.4	21.2	21.3	1.0	-.0049	4.6
1330	94	166	4.9	21.3	21.4	1.1	-.0043	4.6
1400	92	171	5.4	21.5	21.4	1.1	-.0043	4.5
1430	89	172	6.0	21.6	21.2	2.6	-.0026	4.4
1500	87	168	6.0	21.6	21.2	2.6	-.0026	4.6
1530	85	149	6.0	21.6	21.1	3.9	-.0009	4.1
1600	82	138	6.0	21.6	21.1	3.9	-.0009	3.7
1630	80	127	6.0	21.6	21.1	6.0	.0012	3.3
1700	78	113	6.0	21.6	21.1	6.0	.0012	3.0
1730	76	98	6.0	21.5	21.0	7.6	.0035	2.6
1800	74	80	6.0	21.4	21.0	7.6	.0035	2.3
1830	72	65	6.0	21.4	21.0	9.7	.0044	1.9
1900	72	65	6.0	21.2	21.0	9.7	.0044	1.7

TABLE VI

MABL Model Predicted Atmospheric Mixed Layer Quantities-Case 3.

HOUR	Zi	Zlcl	WIND	Th	SST	MLD	TW	Ze
1830	248	333	0.0	19.0	21.2	0.0	0.0000	0.0
1900	242	328	4.3	19.2	21.2	0.0	0.0000	8.1
1930	237	324	4.5	19.3	21.2	0.0	0.0000	8.1
2000	232	320	4.7	19.5	21.2	0.0	0.0000	8.3
2030	227	315	4.9	19.6	21.2	0.0	0.0000	8.4
2100	222	309	5.1	19.8	21.2	0.0	0.0000	8.5
2130	217	303	5.3	19.9	21.2	0.0	0.0000	8.5
2200	213	297	5.5	20.1	21.2	0.0	0.0000	8.7
2230	208	291	5.1	20.2	21.2	0.0	0.0000	8.7
2300	204	284	4.8	20.3	21.2	0.0	0.0000	8.4
2330	199	278	4.4	20.4	21.2	0.0	0.0000	8.0
0000	195	273	4.1	20.4	21.2	0.0	0.0000	7.9
0030	190	269	3.7	20.5	21.2	0.0	0.0000	7.3
0100	186	263	3.4	20.6	21.2	0.0	0.0000	6.9
0130	181	258	3.0	20.6	21.2	0.0	0.0000	6.5
0200	176	254	2.9	20.7	21.2	0.0	0.0000	6.2
0230	172	250	2.8	20.7	21.2	0.0	0.0000	6.0
0300	168	245	2.6	20.8	21.2	0.0	0.0000	5.8
0330	163	240	2.5	20.8	21.2	0.0	0.0000	5.7
0400	159	236	2.6	20.8	21.2	0.0	0.0000	5.5
0430	155	231	2.8	20.8	21.2	0.0	0.0000	5.6
0500	151	226	2.9	20.9	21.2	0.0	0.0000	5.6
0530	147	220	3.0	20.9	21.2	0.0	0.0000	5.7
0600	144	214	2.8	20.9	21.2	0.0	0.0000	5.6
0630	140	210	2.5	20.9	21.2	0.0	0.0000	5.3
0700	136	208	3.3	21.0	21.2	0.0	0.0000	5.0
0730	133	207	3.0	21.0	21.2	0.0	0.0000	4.9
0800	129	206	1.8	21.1	21.2	0.0	0.0000	4.7
0830	126	205	1.5	21.1	21.2	0.0	0.0000	4.5
0900	122	203	1.8	21.1	21.2	0.0	0.0000	4.3
0930	119	202	1.5	21.1	21.2	0.0	0.0000	4.2
1000	115	200	1.4	21.2	21.2	0.0	0.0000	4.2
1030	112	200	3.3	21.2	21.2	0.0	0.0000	4.3
1100	109	196	3.7	21.2	21.2	0.0	0.0000	4.0
1130	106	191	3.1	21.2	21.2	0.0	0.0000	3.9
1200	103	186	3.6	21.3	21.2	0.0	0.0000	3.8
1230	101	179	4.0	21.3	21.2	0.0	0.0000	3.8
1300	98	171	4.4	21.3	21.2	0.0	0.0000	3.8
1330	95	161	4.9	21.4	21.2	0.0	0.0000	3.8
1400	92	153	5.5	21.4	21.2	0.0	0.0000	3.7
1430	90	146	6.0	21.5	21.2	0.0	0.0000	3.7
1500	87	138	6.0	21.5	21.2	0.0	0.0000	3.8
1530	85	130	6.0	21.6	21.2	0.0	0.0000	3.6
1600	83	122	6.0	21.6	21.2	0.0	0.0000	3.6
1630	81	115	6.0	21.6	21.2	0.0	0.0000	3.6
1700	78	106	6.0	21.6	21.2	0.0	0.0000	3.5
1730	76	94	6.0	21.5	21.2	0.0	0.0000	3.4
1800	74	80	6.0	21.5	21.2	0.0	0.0000	3.3
1830	72	69	6.0	21.4	21.2	0.0	0.0000	3.2
1900	71	66	6.0	21.3	21.2	0.0	0.0000	3.1

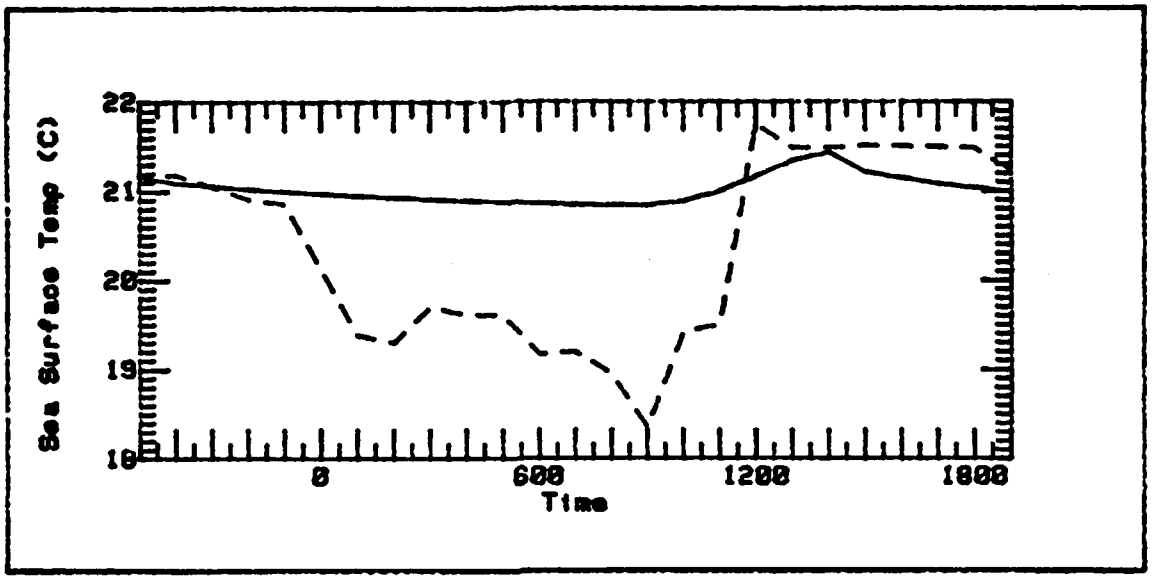

Figure 26. Time Evolution of the Sea-Surface Temperature-Case 3. Predicted values are shown by the solid line. Observed values are shown by the dashed line.

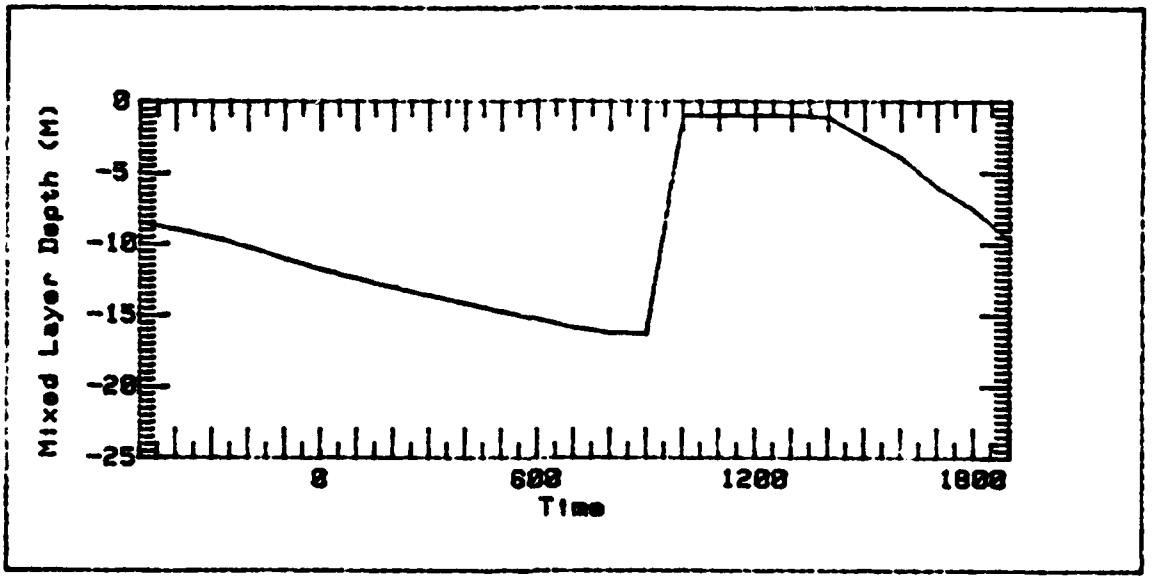

Figure 27. Time Evolution of Ocean Mixed Layer Depth (MLD) - Case 3.

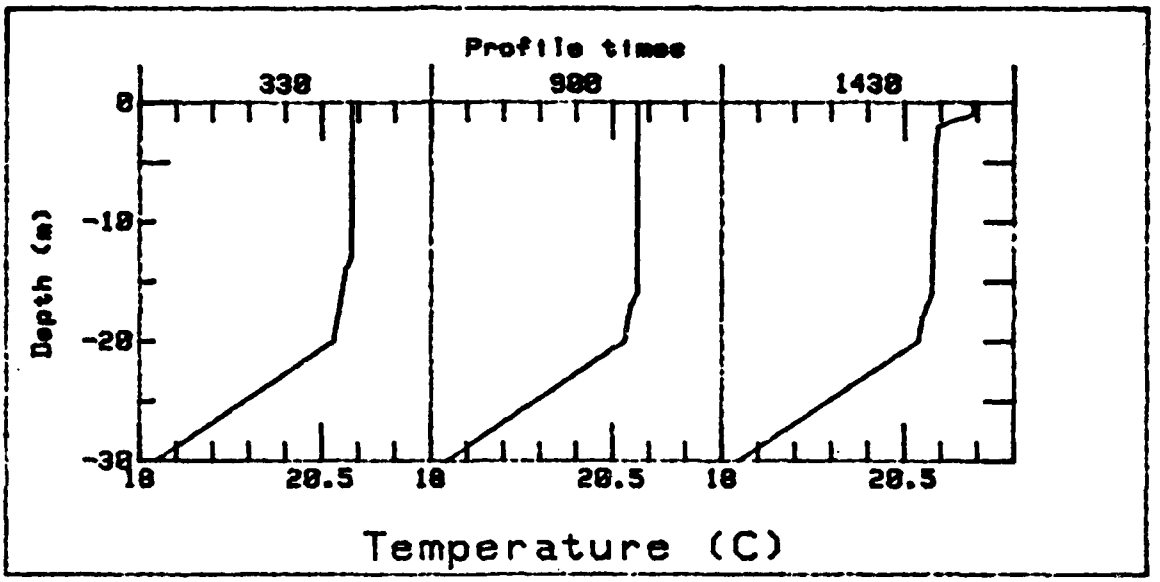

Figure 28. Selected Ocean Vertical Temperature Profiles- Case 3.

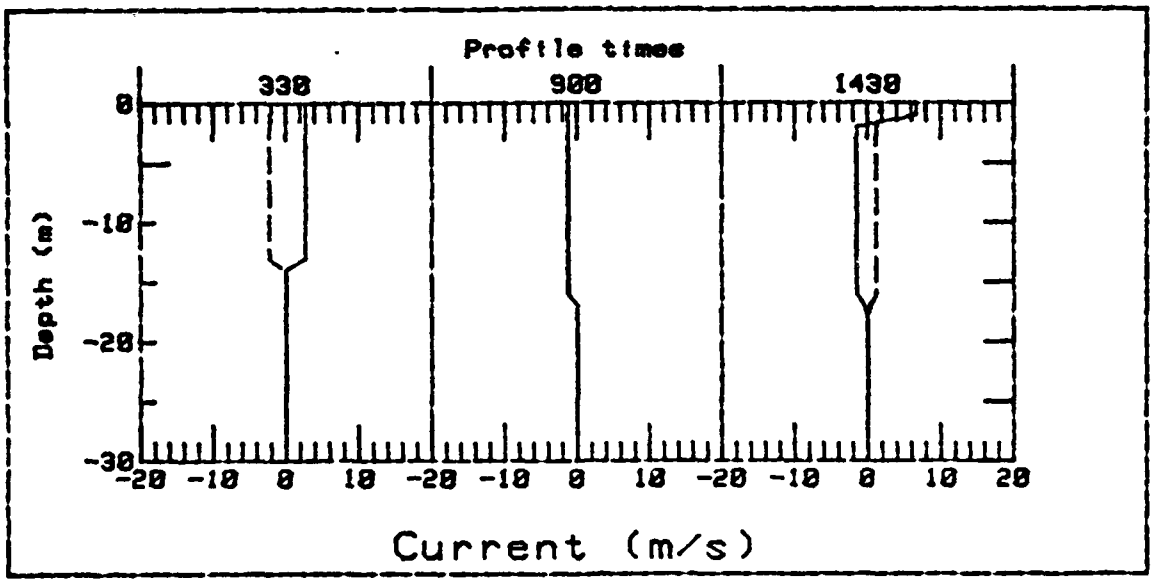

Figure 29. Selected Ocean Vertical Profiles of the Horizontal Wind Driven Currents- Case 3. East-west component u (solid line) North-south component v (dashed).

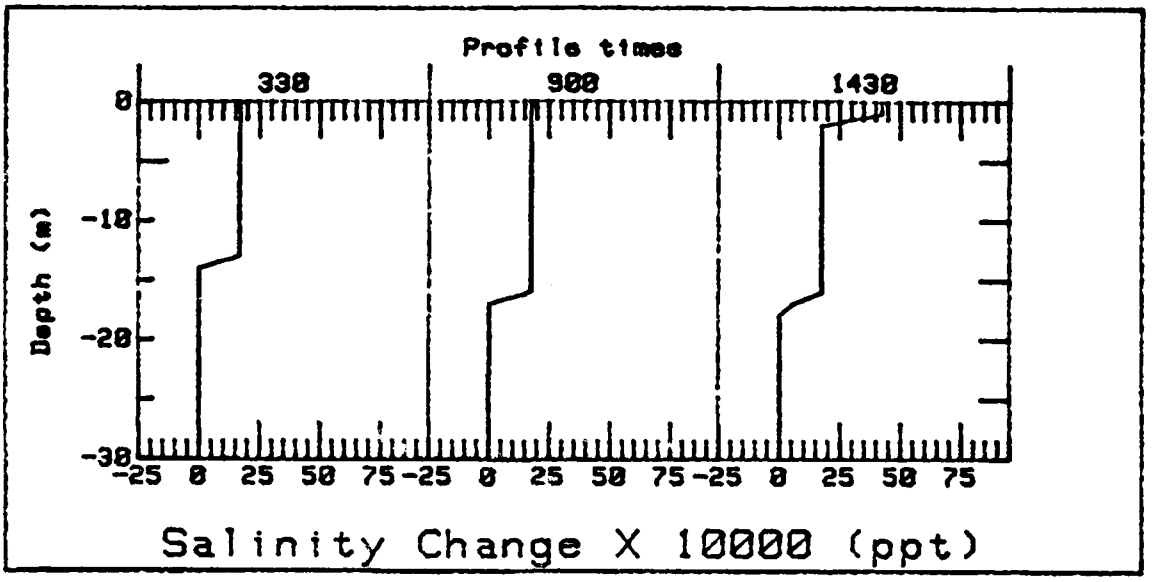

Figure 30. Selected Change in Ocean Vertical Salinity Profiles- Case 3.

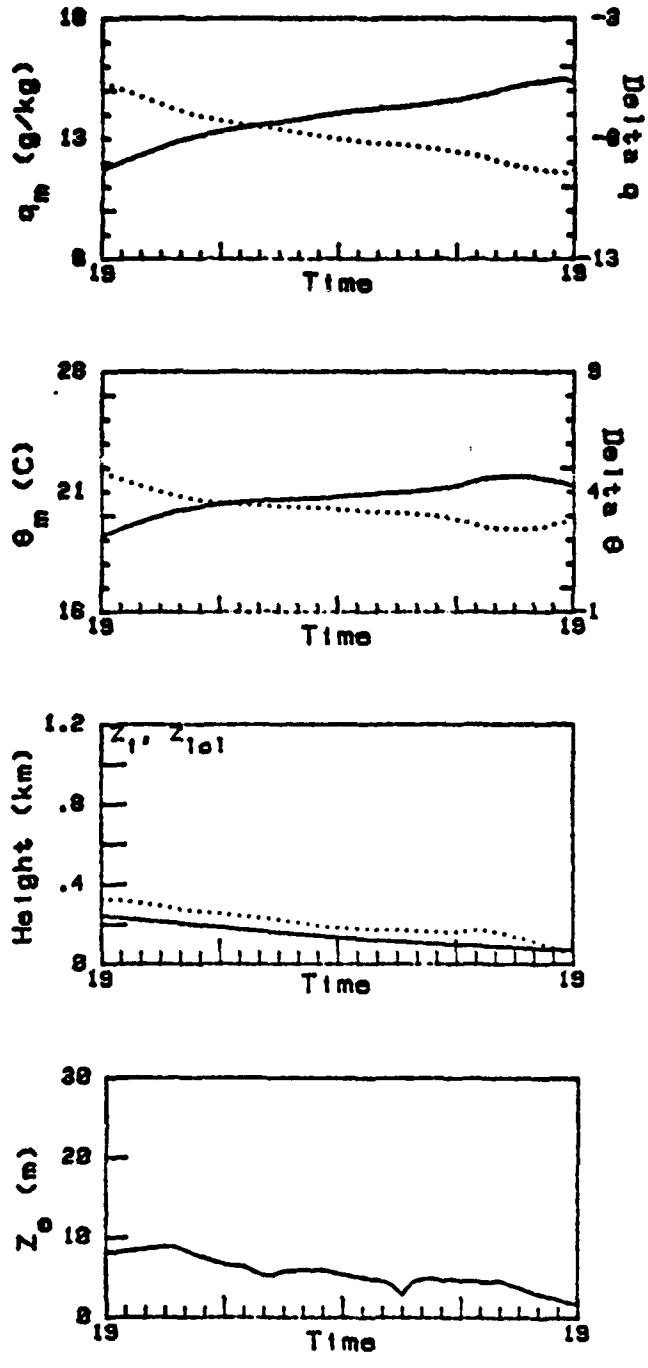

Figure 31. Graphical Display of the Coupled Model Predicted Atmospheric Mixed Layer Quantities- Case 3.

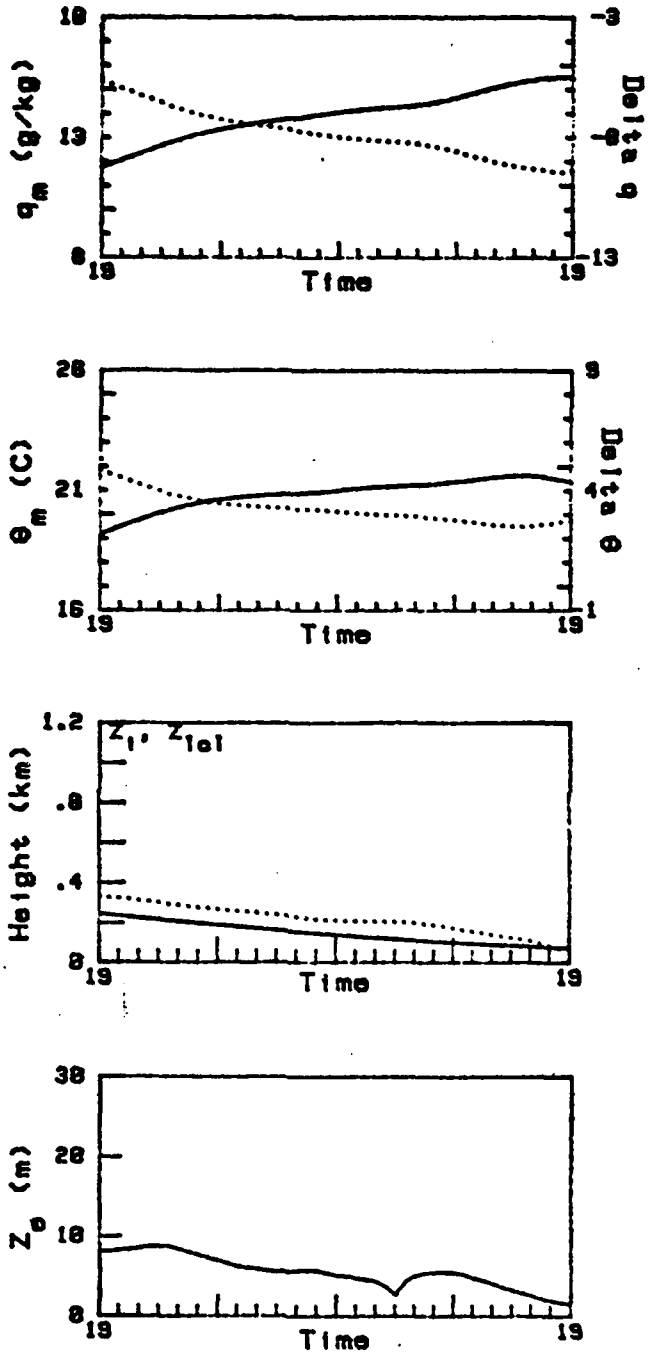

Figure 32. Graphical Display of the MABL Model Predicted Atmospheric Mixed Layer Quantities- Case 3.

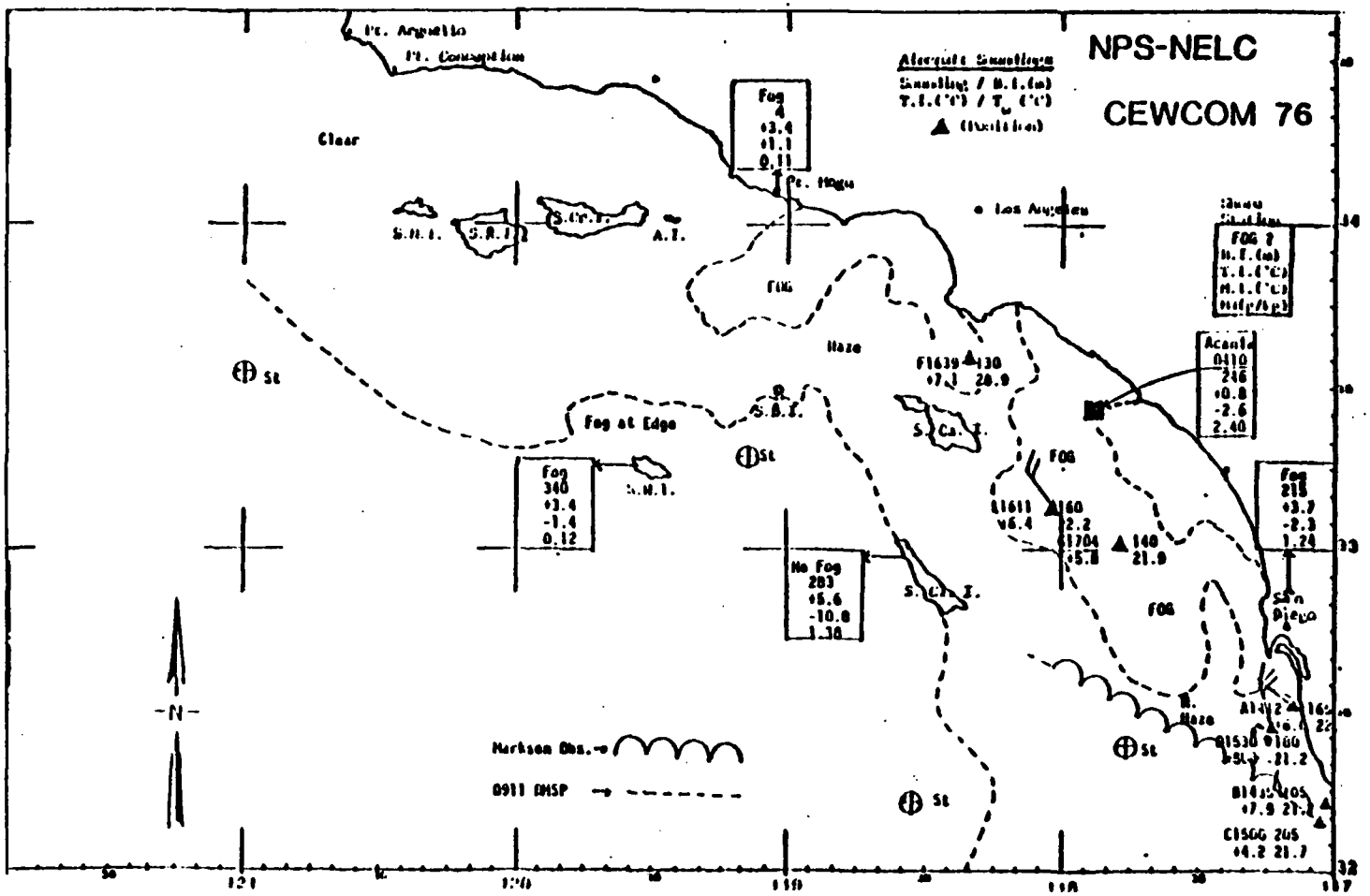

Figure 33. Fog and Stratus Cloud Positions During Case 3 Prediction Period.

LIST OF REFERENCES

Backes, D.A., 1977: "Santa Ana Associated Offshore Fog: Forecasting with a Sequential Model", M.S. Thesis, Naval Postgraduate School, Monterey, CA., 112 pp.

Brower, D.A., 1982: "Marine Atmospheric Boundary Layer and Inversion Forecast Model", M.S. Thesis, Naval Postgraduate School, Monterey, CA., 136 pp.

Davidson, K.L., C.W. Fairall, P. J. Boyle, and G.E. Schacher, 1983: "Verification of an Atmospheric Mixed-Layer Model for a Coastal Region", submitted,CA., 39 pp. J. Appl. Meteor., 28 pp.

Deardorf, J.W., 1979: "Prediction of Convective Mixed Layer Entrainment for Realistic Capping Inversion Structure", J. Atmos. Sci., 36, 424-436.

Fairall, C.W., K.L. Davidson, T. M. Houlihan, and G.E. Schacher, 1977: "Atmospheric Turbulence Measurements in Marine Fog during CEWCOM-76", NPS61-77-004, Naval Postgraduate School, Monterey, CA., 61 pp.

Fairall, C.W., G.E. Schacher, K.L. Davidson, and T.M. Houlihan, 1978: "Atmospheric Marine Boundary Layer Measurements in the Vicinity of San Nicolas Island during CEWCOM-78", NPS61-78-007, Naval Postgraduate School, Monterey, CA., 72 pp.

Fairall, C.W., K.L. Davidson, and G.E. Schacher, 1981: "A Review and Evaluation of Integrated Atmoshperic Boundary-Layer Models", NPS-63-81-004, Naval Postgraduate School, Monterey, CA., 89 pp.

Fleagle, R.G. and J.A. Businger, "An Introduction to Atmospheric Physics." New York, New York: Academic Press, 1978.

Garwood, R.W., Jr., 1977: "An Ocean Mixed Layer Model Capable of Simulating Cyclic States", J. Phys. Oceanogr., 7, 455-468.

Gleason, J.P., 1982: "Single-Station Assessments of the Synoptic-Scale Forcing on the Marine Atmospheric Boundary Layer", M.S. Thesis, Naval Postgraduate School, Monterey, CA., 55 pp.

Husby, D.M. andG.R. Seckel, 1978: "Large Scale Air-Sea Interactions at Ocean Station V", NOAA Tech. Rep. NMFS SSRF-696, 44 pp.

Laevastu, T., 1960: "Factors Affecting the Temperature of Surface Layer of the Ocean", Soc. Scient. Fennica. Comment. Physico.-Mathem., 25(1), 1-136.

Miller, J.R., 1976: "The Salinity Effects in a Mixed Layer Ocean Model", J. Phys. Oceanogr., 6, 29-35.

Seckel, G.R. and F.H. Beaudry, 1973: "The Radiation from Sun and Sky over the North Pacific Ocean", EOS, Trans. Am. Geophys. Union, 54, 1114.

Shook, R.E. 1980: "The One-Dimensionality of the Upper Ocean Mixing and the Role of Advection during the Pole Experiment", M.S. Thesis, Naval Postgraduate School, Monterey, CA., 72 pp.

Siclari, A., 1978: "Sea Surface Thermal Characteristics in the Vicinity of Southern Californias Channel Islands", Department of Oceanography, Naval Postgraduate School, Monterey, CA., 61 pp.

Slingo, A., S. Nicholls, and C.L. Wrench, 1982: "A Field Study of Nocturnal Stratocumulus: III. High Resolution Radiative and Microphysical Observations", Quart. J. R. Met. Soc., 108, 145-166.

Stage, S.A. and J.A. Businger, 1981: "A Model for Entrainment into a Cloud-Topped Marine Boundary Layer- Part I: Model Discription and Application to a Cold Air Outbreak Episode", J. Atmos. Sci., 38, 2213-2229.

Stage, S.A. and J.A. Businger, 1981: "A Model for Entrainment into a Cloud-Topped Marine Boundary Layer- Part II: Discussion of Model Behavior and Comparison with other Models", J. Atmos. Sci., 38, 2230-2242.

Tabata, S., 1964: "A Study of the Main Physical Factors Governing the Oceanographic Conditions of Station P in the Northwest Pacific Ocean", Ph. D. Thesis, University of Tokyo, 264 pp.

Tennekes, H. and A.G.M. Dreidonks, 1981: "Basic Entrainment Equations for the Atmospheric Boundary Layer", Boundary Layer Meteorology, 20, 515-531.

INITIAL DISTRIBUTION LIST

		No. Copies
1.	Defense Technical Information Center Cameron Station Alexandria, VA 22314	2
2.	Library, Code 0142 Naval Postgraduate School Monterey, CA 93940	2
3.	Professor R.J. Renard, Code 63Rd Naval Postgraduate School Monterey, CA 93940	1
4.	Professor C.N.K. Mooers, Code 68Mr Naval Postgraduate School Monterey, CA 93940	1
5.	Professor K.L. Davidson, Code 63Ds Naval Postgraduate School Monterey, CA 93940	10
6.	Professor R.W. Garwood, Code 68Gd Naval Postgraduate School Monterey, CA 93940	4
7.	Mr. P.C. Gallacher, Code 63Ga Naval Postgraduate School Monterey, CA 93940	1
8.	Director Naval Oceanography Division Naval Observatory 34TH and Massachusetts Ave. NW Washington, D.C. 20390	1
9.	Commander Naval Oceanography Command NSTL Station Bay St. Louis, MS 39522	1
10.	Commanding Officer Naval Oceanographic Office NSTL Station Bay St. Louis, MS 39522	1
11.	Commanding Officer Fleet Numerical Oceanography Center Monterey, CA 93940	1

12. Commanding Officer 1
Naval Ocean Research and Development Activity
NSTL Station
Bay St. Louis, MS 39522

13. Commanding Officer 1
Naval Environmental Prediction Research Facility
Monterey, CA 93940

14. Chairman Oceanography Department 1
U.S. Naval Academy
Anapolis, MD 21402

15. Chief of Naval Research 1
800 N. Quincy Street
Arlington, VA 22217

16. Office of Naval Research (Code 480) 1
Naval Oceanography Research and Development Activity
NSTL Station
Bay St. Louis, MS 39522

17. Scientific Liaison Office 1
Office of Naval Research
Scripps Institute of Oceanography
La Jolla, CA 92037

18. Library 1
Scripps Institute of Oceanography
P.O. Box 2367
La Jolla, CA 92037

19. Library 1
Department of Oceanography
University of Washington
Seattle, WA 98105

20. Library 1
CICESE
P.O. Box 4803
San Ysidro, CA 92073

21. Library 1
School of Oceanography
Oregon State University
Corvallis, OR 97331

22. Commander 1
Oceanographic Systems Pacific
Box 1390
Pearl Harbor, HI 96860

23. Commanding Officer — 2
Attn:
CDR D. Hinsman
Dr. A. Weinstein
Naval Environmental Prediction Research Facility
Monterey, CA ; 93940

24. CDR J. J. Jensen, USN, Code 5E731 — 1
Office of Assistant Secretary of the Navy
Assistant for Environmental Science
Washington, DC 20360

25. Commanding Officer — 1
Attn:
LT T. McPherson
COMNAVSOUTH
BOX 168
FPO NEW YORK 09524

26. Commanding Officer — 1
Attn:
LT. M. C. O'Loughlin
Naval Eastern Oceanography Center
Naval Air Station
Norfolk, VA 23511

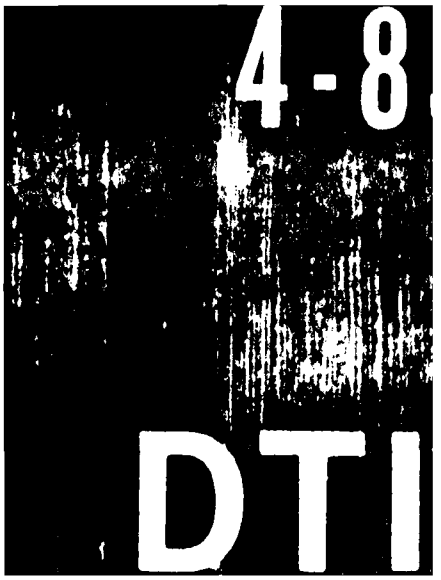
4-8
DTI